Acta Pharmacologica Sinica

www.nature.com/aps

ARTICLE

# Corynoxine B derivative CB6 prevents Parkinsonian toxicity in mice by inducing PIK3C3 complex-dependent autophagy

Zhou Zhu[1,2,3], Liang-feng Liu[1,4], Cheng-fu Su[1,2,3], Jia Liu[1,2,3], Benjamin Chun-Kit Tong[1,2,3], Ashok Iyaswamy[1,2,3], Senthilkumar Krishnamoorthi[1,2,3], Sravan Gopalkrishnashetty Sreenivasmurthy[1,2,3], Xin-jie Guan[1,2,3], Yu-xuan Kan[1,2,3], Wen-jian Xie[2], Chen-liang Zhao[2], King-ho Cheung[1,2,3], Jia-hong Lu[5], Jie-qiong Tan[6], Hong-jie Zhang[2], Ju-xian Song[1,7] and Min Li[1,2,3]

Increasing evidence shows that autophagy impairment is involved in the pathogenesis and progression of neurodegenerative diseases including Parkinson's disease (PD). We previously identified a natural alkaloid named corynoxine B (Cory B) as a neuronal autophagy inducer. However, its brain permeability is relatively low, which hinders its potential use in treating PD. Thus we synthesized various derivatives of Cory B to find more potent autophagy inducers with improved brain bioavailability. In this study, we evaluated the autophagy-enhancing effect of CB6 derivative and its neuroprotective action against PD in vitro and in vivo. We showed that CB6 (5–40 μM) dose-dependently accelerated autophagy flux in cultured N2a neural cells through activating the PIK3C3 complex and promoting PI3P production. In $MPP^+$-treated PC12 cells, CB6 inhibited cell apoptosis and increased cell viability by inducing autophagy. In MPTP-induced mouse model of PD, oral administration of CB6 (10, 20 mg· $kg^{-1}$. $d^{-1}$, for 21 days) significantly improved motor dysfunction and prevented the loss of dopaminergic neurons in the striatum and substantia nigra pars compacta. Collectively, compound CB6 is a brain-permeable autophagy enhancer via PIK3C3 complex activation, which may help the prevention or treatment of PD.

**Keywords:** autophagy; Parkinson's disease; PIK3C3 complex; PI3P; dopaminergic neuron; $MPP^+$; corynoxine B; oxindole alkaloid

*Acta Pharmacologica Sinica* (2022) 43:2511–2526; https://doi.org/10.1038/s41401-022-00871-0

## INTRODUCTION

Parkinson's disease (PD) is a progressive neurodegenerative disease with clinical symptoms of motor disturbances [1]. The neuropathological hallmarks of PD are the loss of dopaminergic nigrostriatal neurons and the presence of Lewy bodies composed of alpha-synuclein (SNCA) [2]. Currently available drugs for PD patients, primarily dopamine agonists, relieve the motor symptoms but do not prevent or reverse the progressive loss of dopaminergic neurons [3]. Thus, the discovery of disease-modifying drugs which can stop the progression of PD is urgently needed [3].

Macroautophagy (henceforth referred to as autophagy) is an evolutionarily conserved cellular process [4]. During the process, autophagosomes fuse with lysosomes to degrade and recycle cellular components, which include toxic aggregate-prone proteins, impaired organelles, and invading pathogens [4, 5]. Accumulating evidence implicates autophagy dysfunction in the pathogenesis and progression of neurodegenerative diseases including PD [6, 7]. Specifically, pathological studies have demonstrated the decreased levels and activity of autophagy-regulatory proteins in postmortem PD brains [8, 9]. Besides, genetic studies revealed that mutation of some genes, including SNCA, LRRK2, and VPS35, could downregulate autophagy and lead to the increased risk of familial or sporadic PD [10–13]. Moreover, autophagy-deficient mice with *Atg5*- or *Atg7*-knockout are easier to develop some PD-like symptoms including motor dysfunction and the formation of inclusion bodies [14, 15]. Given that autophagy dysfunction is closely related to the pathogenesis of PD, restoration of autophagy may be a promising strategy for treating PD [6, 16, 17].

Corynoxine B (Cory B) is a natural oxindole alkaloid isolated from the Chinese herbal 1medicine *Uncaria rhynchophylla* (Miq.) Jacks (钩藤 in Chinese) that has been used for the treatment of PD-related symptoms [18, 19]. In previous studies, we found that Cory B induced autophagy by regulating different pathways [20–22]. To develop more potent autophagy inducers with good brain bioavailability, we synthesized various derivatives of Cory B and tested their autophagy-inducing potency. A derivative termed CB6, which has an N-propyl group modified on Cory B to improve the hydrophobicity, showed similar autophagy-inducing effects and improved brain permeability. In this study, we determined the molecular mechanisms by which CB6 induces autophagy and examined its neuroprotective effects in cellular and animal models of PD. We found that CB6 induced autophagy via enhancing the activity of PIK3C3/VPS34 complex. In a 1-methyl-4-phenylpyridinium ($MPP^+$)-induced PC12 cell model of PD,

[1]Mr. & Mrs. Ko Chi-Ming Centre for Parkinson's Disease Research, School of Chinese Medicine, Hong Kong Baptist University, Hong Kong, SAR, China; [2]School of Chinese Medicine, Hong Kong Baptist University, Hong Kong, SAR, China; [3]Institute for Research and Continuing Education, Hong Kong Baptist University, Shenzhen 518057, China; [4]Limin Pharmaceutical Factory, Livzon Group Limited, Shaoguan 512028, China; [5]State Key Laboratory of Quality Research in Chinese Medicine, Institute of Chinese Medical Sciences, University of Macau, Macau, SAR, China; [6]Center for Medical Genetics and Hunan Key Laboratory of Animal Model for Human Diseases, School of Life Sciences, Central South University, Changsha 410078, China and [7]Medical College of Acupuncture-Moxibustion and Rehabilitation, Guangzhou University of Chinese Medicine, Guangzhou 510006, China
Correspondence: Ju-xian Song (juxian.song@gmail.com) or Min Li (limin@hkbu.edu.hk)

Received: 12 July 2021 Accepted: 17 January 2022
Published online: 25 February 2022

CB6 induced autophagy to inhibit cell apoptosis and restore cell viability. Furthermore, oral administration of CB6 induced autophagy in mouse brains and prevented the loss of dopaminergic neurons in a 1-methyl-4-phenyl-1,2,3,6-tetrahydropyridine (MPTP) mouse model of PD.

## MATERIALS AND METHODS

### Reagents and antibodies

CB6 was synthesized by reacting Cory B (APC-459, Aktin, Chengdu, China) with iodine propane in dimethylformamide (DMF); it was purified by silica gel chromatography, achieving ~98% purity. Anti-tyrosine hydroxylase (TH) (AB152) antibody was purchased from Millipore (Burlington, MA, USA). Anti-ACTB/β-actin (sc-47778) and anti-UB/Ubiquitin (sc-8017) antibodies were purchased from Santa Cruz (Dallas, TX, USA). Anti- SQSTM1/p62 (P0067) antibody, $MPP^+$ iodide (D048), MPTP hydrochloride (M0896), cycloheximide (CHX) (C1988), chloroquine (CQ) (C6628), and 3-methyladenine (3-MA) (M9281) were purchased from Sigma-Aldrich (St. Louis, MO, USA). Dopamine hydrochloride (PHR1090), 3,4-dihydroxyphenylacetic acid (DOPAC) (11569), and homovanillic acid (HVA) (69673) were purchased from Supelco (Sigma-Aldrich, St. Louis, MO, USA). Anti-LC3B (NB100-2220) antibody was purchased from Novus Biologicals (Littleton, CO, USA). Anti-ATG7 (sc-8558), anti-phospho-MTOR (Ser2448) (5536), anti-MTOR (2983), anti-phospho-RPS6KB1/P70S6K (Thr389) (9205), anti-RPS6KB1/P70S6K (9202), anti-phospho-EIF4EBP1 (Thr37/46) (2855), anti-EIF4EBP1 (9644), anti-phospho-ULK1 (Ser757) (14202), anti-ULK1 (8054), anti-TSC2 (4308), anti-cleaved PARP1 (Asp214) (94885), anti-cleaved CASP3 (Asp175) (9661), anti-CASP3 (14220) antibodies were purchased from Cell Signaling Technology (Danvers, MA, USA). Anti-PARP1 (A0942) antibody was purchased from ABclonal (Woburn, MA, USA). Protein G magnetic beads (10003D) were purchased from Invitrogen (Waltham, MA, USA). HRP-conjugated goat anti-mouse IgG (115-035-003) and goat anti-rabbit IgG (111-035-144) secondary antibodies were purchased from Jackson ImmunoResearch Laboratories (West Grove, PA, USA). Alexa Fluor® 594 goat anti-rabbit IgG (A-11012) was purchased from Life Technologies (Carlsbad, CA, USA). Bafilomycin A1 (Baf A1) (S1413) and SAR405 (S7682) were purchased from Selleckchem (Houston, TX, USA). Torin 1 (2273) was purchased from BioVision (Milpitas, CA, USA). Spautin1 (HY-12990) was purchased from MedChemExpress (Monmouth Junction, NJ, USA). Actinomycin D (ActD) (11421) was purchased from Cayman (Ann Arbor, MI, USA). *Atg7* (mouse) siRNA (L-049953-00-0005), *Becn1* (mouse) siRNA (L-055895-00-0005), *TSC2* (human) siRNA (L-003029-00-0005), and non-target siRNA were purchased from Dharmacon (Lafayette, CO, USA).

### Cell culture and drug treatment

Neuro-2a (N2a) cells, PC12 cells, HEK 293 cells, and HeLa cells were maintained in DMEM (11965084, Gibco, Waltham, MA, USA) supplemented with 10% FBS (10500064, Gibco, Waltham, MA, USA). All the cells were grown at 37 °C in a humid incubator supplied with 5% $CO_2$. For Torin 1 treatment, cells were treated with 250 nM Torin 1 for 5 h to inhibit MTORC1 pathway and for 12 h to induce autophagy. For Baf A1 treatment, 100 nM Baf A1 was used for 3 h to inhibit autophagosome-lysosome fusion. For CQ treatment, 100 μM CQ was used for 3 h or 24 h to inhibit lysosomal degradation. For 3-MA treatment, 5 mM 3-MA was added to treat cells for 30 min before CB6 treatment to inhibit the activity of the PIK3C3 complex. For SAR405 treatment, 5 μM SAR405 was added to treat cells for 30 min before CB6 treatment to inhibit the activity of the PIK3C3 complex. For Spautin1 treatment, 10 μM SAR405 was added to treat cells for 30 min before CB6 treatment to inhibit deubiquitination of the PIK3C3 complex. For CHX treatment, 5 μg/mL CHX was used for 14 h to inhibit protein synthesis. For ActD treatment, 0.1 μM ActD was used for 24 h to inhibit RNA synthesis. For $MPP^+$ treatment, 0.125–4 mM $MPP^+$ were used for 48 h treatment to establish a cellular model of PD.

### Cell transfection

For overexpression experiments, cells were transfected with indicated plasmids using Lipofectamine 3000 reagent (L3000015, Invitrogen, Waltham, MA, USA). The plasmids were mixed and incubated with Lipofectamine 3000 in Opti-MEM medium (31985070, Gibco, Waltham, MA, USA) for 20 min at room temperature. The mixture was added to N2a/HEK 293 cells and cultured for 24 h, followed by treatment with the indicated drugs. For knockdown experiments, cells were transfected with indicated siRNAs using Lipofectamine RNAiMAX reagent (13778030, Invitrogen, Waltham, MA, USA). The siRNAs were mixed and incubated with Lipofectamine RNAiMAX in Opti-MEM medium for 20 min at room temperature. The mixture was added to N2a/HeLa cells and cultured for 60 h, followed by treatment with the indicated drugs.

### Lactate dehydrogenase (LDH) release assay

N2a cells were seeded into 24-well plates. After 24-h incubation, the cells were treated with different concentrations of CB6 for 24 h. After drug treatments, the culture media was collected and centrifuged. LDH kits (11644793001, Roche, Basel, Switzerland) were used for the measurement of LDH levels in the supernatants according to the manufacturer's protocol. To calculate the cytotoxicity, cells treated without any compound were used as negative controls; cells treated with 1% Triton X-100 were used as positive controls.

### AlamarBlue assay

AlamarBlue™ Cell Viability Reagent (DAL1025, Invitrogen, Waltham, MA, USA) was used to determine the cell viability of $MPP^+$-treated PC12 cells. PC12 cells were seeded into 48-well plates (250 μL medium each well) and treated with indicated drugs. After drug treatments, 25 μL alamarBlue™ reagent was directly added to the culture medium of each well. The plates were mixed well and incubated at 37 °C for 1 h. The absorbance value of the alamarBlue reagent was monitored at 570 nm, using 600 nm as a reference wavelength.

### Western blotting

Cells were seeded into 12-well plates and treated with indicated drugs. After washing with ice-cold PBS twice, cells were lysed in RIPA lysis buffer (9803, Cell Signaling Technology, Danvers, MA, USA) with protease inhibitors (HY-K0011, MedChemExpress, Monmouth Junction, NJ, USA) and phosphatase inhibitors (A32957, Pierce, Waltham, MA, USA). After the lysates were sonicated and centrifuged at 15,000 r/min for 30 min at 4 °C, the protein concentrations of the supernatants were determined by BCA assay (23225, Pierce, Waltham, MA, USA). Protein lysates were adjusted to the same concentration with loading buffers and boiled for 10 min at 70 °C. The samples were cooled on ice and loaded on 12% SDS-PAGE gels. After being separated on the gels, the samples were transferred onto 0.45 μm PVDF membranes, blocked with 5% non-fat milk in TBST, and incubated with primary antibodies overnight at 4 °C. Then, the membranes were incubated with secondary antibodies for 2 h at room temperature. The protein chemiluminescence signals were detected by ECL kits (34580, SuperSignal, Waltham, MA, USA) and captured on X-ray film (FUMINGWEI, Shenzhen, China).

### Transmission electron microscopy (TEM)

N2a cells were seeded into 90 mm dishes, grown to 60% confluence, and then treated with CB6 (20 μM) for 14 h. Immediately after the culture medium was discarded, cells were fixed with 2.5% glutaraldehyde (G5882, Sigma-Aldrich, St. Louis, MO, USA) in 0.1 M sodium cacodylate buffer (11654, Electron Microscopy Sciences, Hatfield, PA, USA) for 1 h at room

temperature. After being fixed, the cells were scraped, centrifuged, and rinsed with 0.1 M sucrose in cacodylate buffer. Cells were post-fixed in 1% osmium tetroxide ($OsO_4$) and dehydrated. After being embedded in Poly/Bed® 812, the samples were cut into 100 nm ultra-thin sections by ultramicrotome. Then the sections were examined on a Philips CM100 transmission electron microscope at the University of Hong Kong.

Immunofluorescence staining
After transfections or drug treatments, cells on the coverslips were fixed in 4% paraformaldehyde (PFA) in PBS for 15–20 min at room temperature, permeabilized in 0.25% ice-cold Triton X-100 for 10 min, blocked with 2% BSA for 1 h, and incubated with primary antibody overnight at 4 °C. On the second day, the cells were stained with fluorescent secondary antibodies for 2 h at room temperature and stained with DAPI for 3–5 min. Then the coverslips were mounted on slides and air-dried. A confocal microscope (Leica TCS SP8, Weitzlar, Germany) was used to acquire cell images.

Quantification of phosphatidylinositol 3-phosphate (PI3P)
N2a cells were seeded into 90 mm dishes, grown to 80% confluence, and then treated with CB6 (20 μM) for 6 h. Cells were lysed in Nonidet P-40 (NP-40) cell lysis buffer containing 25 mM Tris (J75825, Thermo Scientific, Waltham, MA, USA), pH 7.6, 100 mM NaCl (J21618-A7, Thermo Scientific, Waltham, MA, USA), 0.5% NP40 (74385, Sigma-Aldrich, St. Louis, MO, USA), 1 mM EDTA (E9884, Sigma-Aldrich, St. Louis, MO, USA), 10% glycerol (15514-011, Invitrogen, Waltham, MA, USA) with protease inhibitors. Anti-BECN1 antibody (sc-10086, Santa Cruz, Dallas, TX, USA) or IgG antibody (10500 C, Invitrogen, Waltham, MA, USA) was used to immunoprecipitate the PIK3C3 complex. The PIK3C3 kinase reaction was performed and the quantification of PI3P level was determined by using a Class III PI3-Kinase Kit (K-3000, Echelon Biosciences, Salt Lake City, UT, USA) according to the manufacturer's protocol.

Triton X-100-soluble and -insoluble fractionation
After the indicated drug treatments, PC12 cells were lysed with 1% Triton X-100 (T9284, Sigma-Aldrich, St. Louis, MO, USA) in PBS with protease inhibitors on ice for 30 min and centrifuged at 15,000 r/min for 30 min at 4 °C. After centrifugation, the supernatants were collected as Triton X-100-soluble fractions. The pellets were washed twice with 1% Triton X-100 in PBS and further lysed with 1% SDS and 1% Triton X-100 in PBS at 60 °C for 1 h. Lysates were centrifuged at 15,000 r/min for 30 min and the supernatants were collected as Triton X-100-insoluble fractions. Protein samples were subjected to Western blot analysis as described above.

Animals
Two-month-old male C57BL/6 mice were purchased from the Chinese University of Hong Kong and acclimated for at least one week before experiments. All the mice used for the study were maintained under 12 h light or dark cycles and were provided *ad libitum* access to chow and water. For autophagy-inducing experiments, mice ($n = 3$ or 4) were treated with oral administration of vehicle or CB6 (10 mg/kg or 20 mg/kg) for 7 consecutive days. For MPTP mouse model experiments, two-month-old male C57BL/6 mice were randomly separated into four groups ($n = 10$): Saline group; MPTP group (MPTP-30 mg/kg); MPTP + CB6-10 group (MPTP-30 mg/kg + CB6-10 mg/kg) and MPTP + CB6-20 group (MPTP-30 mg/kg + CB6-20 mg/kg). Mice received MPTP ($30\ mg \cdot kg^{-1} \cdot d^{-1}$ free base) intraperitoneally (i.p.) for 7 consecutive days. The first dosage of CB6 treatment was orally administered one week before the first injection of MPTP and CB6 treatment continued for 21 consecutive days. MPTP hydrochloride (M0896, Sigma-Aldrich, St. Louis, MO, USA) was dissolved in normal saline and CB6 was suspended in 0.5% carboxymethylcellulose sodium (CMC-Na, C5678, Sigma-Aldrich, St. Louis, MO, USA). All the animal experiments were approved by the Hong Kong Baptist University Committee on the Use of Human and Animal Subjects in Teaching and Research.

Rotarod test
A rotarod cylinder was chosen to assess mouse motor coordination (SeDaCom v2.0.000, Harvard apparatus, Holliston, MA, USA). For all tests, mice were brought into the experimental room 30 min before testing. Before MPTP treatment, mice were trained on the rotarod for 3 consecutive days at speeds of 5, 10, and 15 r/min, respectively. Each mouse had 3 trials per day with a 60-min interval between trials. For the test on day 13, the rotarod was accelerated from 4 to 40 r/min within 5 min. A cut-off time of 3 min and an inter-trail interval of 60 min were used. Each mouse was tested three times and the latency to fall was recorded.

Immunohistochemistry
Mice were perfused intracardially with 4% PFA in PBS. Then the brains were removed, post-fixed with 4% PFA overnight in 50 mL tubes, and dehydrated sequentially in 15% and 30% sucrose in PBS. The brains were frozen with Cryomatrix (6769006, Thermo Scientific, Waltham, MA, USA) and sectioned into 25 μm slices by using a microtome (Cryostar NX70, Thermo Scientific, Waltham, MA, USA). Frozen sections of striatum and substantia nigra were collected and stored in 0.4% Triton X-100 at 4 °C. For DAB staining, brain sections were incubated with 3% $H_2O_2$ for 10 min to quench the endogenous peroxidase activity. The sections were blocked with 2% BSA and incubated with anti-TH antibody overnight at 4 °C. Then, the sections were incubated with ABC Elite Kit (PK-6101, Vector Laboratories, Burlingame, CA, USA) and visualized by DAB peroxidase (SK-4100, Vector Laboratories, Burlingame, CA, USA).

Measurement of striatal Dopamine, DOPAC, and HVA levels
The striatum was weighed and homogenized in 500 μL ice-cold 80% methanol in $H_2O$. After centrifugation at $12,000 \times g$ for 20 min at 4 °C, the supernatants were dried under vacuum centrifugation and resolved in 0.2% formic acid in deionized $H_2O$ containing $D_4$-dopamine as an internal standard. After centrifugation at $21,000 \times g$ for 10 min at 4 °C, the supernatants were collected and analyzed with a high-performance liquid chromatography (HPLC) system. UPLC BEH C18 column (1.7 μm particle size, 2.1 mm I.D. × 100 mm, Waters Acquity, Milford, MA, USA) connected with VanGuard Pre-column (2.1 mm I.D. × 5 mm length) was used to determine dopamine and its metabolites. The mobile phase contained 0.2% formic acid in $H_2O$ as mobile phase A and acetonitrile as mobile phase B; the flow rate was 0.3 mL/min. The contents of dopamine and its metabolites were detected by mass spectrometry (MS) for quantification using multiple reaction monitoring. For dopamine, its precursor ion with *m/z* value of 154.1 and product ions of 137.1 and 119.1 were used. For $D_4$-dopamine, its precursor ion with *m/z* value of 158.1 and a product ion of 141.1 were used. For DOPAC, its precursor ion with *m/z* value of 168.1 and a product ion of 123.0 were used. For HVA, its precursor ion with *m/z* of 182.1 and a product ion of 137.0 were used.

Statistical analysis
All data are presented as mean ± SEM. Data were analyzed by unpaired *t*-test or one-way analysis of variance (ANOVA) followed by Dunnett's multiple comparison test, by using GraphPad Prism 7.0 (GraphPad, San Diego, CA, USA). A probability value of $P < 0.05$ was considered statistically significant.

## RESULTS

CB6 has better brain permeability than Cory B
CB6 was synthesized from Cory B with an N-propyl substituent (Supplementary Fig. S1a), and its structure was confirmed by

nuclear magnetic resonance (NMR) spectroscopy (Supplementary Fig. S1e). Due to the addition of the propyl group, CB6 should be more hydrophobic and brain permeable than Cory B. To compare the brain bioavailability of CB6 with Cory B, a brain permeability study was done on C57BL/6 mice through oral administration. At early time points, there was more amount of CB6 in brains but less amount in the plasma compared with that of Cory B (Supplementary Fig. S1b, c). Comparison of compound concentration in brains with that in plasma showed that a larger proportion of CB6 remained in brains than Cory B (Supplementary Fig. S1d), possibly reducing its side effects on other internal organs. Moreover, the peak concentration of CB6 in brains was much higher than Cory B (Supplementary Fig. S1c). In summary, CB6 is easier to pass through the blood-brain barrier (BBB) compared with Cory B.

CB6 promotes autophagy flux in cultured cells

Then we determined the autophagy-inducing effects of CB6 in vitro. Firstly, an LDH release assay was used to detect the cytotoxicity of CB6 on N2a cells (Fig. 1a). MAP1LC3B (LC3B) is a widely used marker of autophagy. LC3B-I is normally localized in the cytosol. Upon autophagy activation, LC3B-I is lipidated to LC3B-II, which associates with autophagosome membranes [23]. Another marker of autophagy, SQSTM1/p62, is an adaptor protein, which connects LC3B and ubiquitinated protein aggregates for the degradation by autophagy [24]. To detect whether CB6 induces autophagy, N2a cells were treated with different concentrations of CB6. The results showed that both 20 μM and 40 μM CB6 significantly increased LC3B-II levels and reduced SQSTM1 levels (Fig. 1b–d), suggesting CB6 induces autophagy. Because 40 μM CB6 tends to be toxic although it was not statistically significant (Fig. 1a), we chose 20 μM for the most subsequent experiments. Then, we found CB6 also induces autophagy in a time-dependent manner, as shown by the increased LC3B-II levels and decreased SQSTM1 levels (Fig. 1e±g). The autophagy-inducing effects of CB6 were further confirmed in PC12 (Supplementary Fig. S2a, b), HeLa (Supplementary Fig. S2c, d), and HEK 293 cells (Supplementary Fig. S2e). In these cells, LC3B-II levels were also increased after CB6 treatment. MTORC1 (a negative regulator of autophagy) inhibitor Torin 1 was used as a positive control to induce autophagy [25, 26]. Moreover, CB6 increased the formation of GFP-LC3 puncta in HeLa cells, indicating an increased level of lipidated LC3B (Supplementary Fig. S2f, g). To visualize the induction of autophagy, we used TEM and found more autophagic vacuoles (double or multi-membrane structures with more electron-dense contents) in CB6-treated N2a cells, compared with control cells (Fig. 1h, i). As ATG7 is involved in the lipidation of LC3B [27], we detected whether knocking down *Atg7* with siRNA reduces CB6-induced lipidation of LC3B. The results showed that LC3B-II levels were increased by CB6 treatment, but it was partially blocked by knocking down *Atg7* (Fig. 1j–l). Overall, these results indicate that CB6 enhances the induction of autophagy.

In fact, lipidated LC3B-II can be accumulated by either autophagy inducers or inhibitors. To further confirm that whether CB6 promotes autophagy flux, cells were treated with CB6 in the presence or absence of lysosomal inhibitors, Baf A1 or CQ, which are widely used for detecting autophagy flux [28]. We found Baf A1 cotreatment further enhanced the increase in LC3B-II levels and restored SQSTM1 levels in CB6-treated cells (Fig. 2a–c). In addition, cotreatment with CQ also enhanced the accumulation of LC3B-II (Fig. 2d–f). In the immunostaining images, greater area and more puncta of GFP-LC3 were formed in CQ-cotreated cells, showing that the degradation of CB6-increased LC3 was further blocked by CQ treatment (Fig. 2g, h). Furthermore, CB6-induced autophagy flux was also confirmed by the significantly increased red-only puncta (autolysosomes) in N2a cells, which were transfected with mRFP-GFP-LC3 plasmids (tandem fluorescent LC3, tfLC3) (Fig. 2i, j). Conversely, autophagy inhibitor CQ did not increase the red puncta number in merged images (Fig. 2i, j). These results further confirm that CB6 induces autophagy flux.

CB6-induced autophagy is independent of the MTORC1 pathway

MTORC1 is well-established as a negative regulator of autophagy, whose activity can be determined by the phosphorylation of its substrates including RPS6KB1 and EIF4EBP1 [29, 30]. Therefore, we firstly wanted to detect whether CB6 regulates the activity of the MTORC1 pathway. To explore this, we firstly treated N2a cells with different concentrations of CB6 for 12 h and found that there was no statistical change in the phosphorylation levels of MTOR and its substrate EIF4EBP1 after CB6 treatment (Fig. 3a–c). However, MTOR inhibitor Torin1 totally eliminated the phosphorylation levels of phosphorylated MTOR, RPS6KB1, and EIF4EBP1 (Fig. 3a–d). Although CB6 decreased the phosphorylation levels of another MTORC1 substrate RPS6KB1, the decrease was very slight when compared with that in cells treated with Torin1 (Fig. 3d). Because MTORC1 negatively regulates autophagy via phosphorylating ULK1 at the Ser757 site, we also detected the phosphorylated ULK1 levels. The results showed that different concentrations of CB6 did not change the phosphorylated ULK1 levels (Fig. 3a, e), indicating the MTORC1 pathway may not mediate CB6-induced autophagy in N2a cells. Moreover, we also treated N2a cells with 20 μM CB6 for different durations. CB6 did not change the phosphorylation levels of MTOR, EIF4EBP1, and ULK1. Only after 12-h treatment, CB6 statistically reduced the phosphorylated RPS6KB1 levels, but mildly when compared with Torin1 treatment (Fig. 3f–j). These results indicated that CB6 partially inhibited MTORC1 pathway in N2a cells. Nevertheless, when we treated PC12 cells with different concentrations of CB6, all the phosphorylation levels of the MTORC1 pathway were unchanged after CB6 treatment, indicating CB6 does not influence the activity of MTORC1 pathway in PC12 cells (Supplementary Fig. S3a). Till now, we have found that CB6 partially inhibits the MTORC1 pathway in N2a cells, but not in dopaminergic PC12 cells, although CB6 induces autophagy in both cells. To further identify whether the inhibition of MTORC1 pathway is involved in the CB6's autophagy-enhancing effects, we knocked down *TSC2* in HeLa cells to activate the MTORC1 pathway and found that the phosphorylated levels of RPS6KB1 increased significantly but they were not reduced after CB6 treatment (Supplementary Fig. S3b). CB6 still successfully increased LC3B-II levels in the MTORC1 pathway-activating cells (Supplementary Fig. S3b). From these results, we conclude that CB6-induced autophagy is not through inhibiting the MTORC1 pathway.

CB6 induces autophagy by activating the PIK3C3 complex

Since CB6 was synthesized from Cory B and we previously reported that Cory B can induce BECN1-dependent autophagy [20], we hypothesized that CB6-induced autophagy is dependent on the PIK3C3 complex. This complex comprises BECN1 and plays a significant role in the lipidation of LC3B and the initiation of autophagy flux [31, 32]. First, we found that *Becn1* knockdown impaired LC3B-II upregulation following CB6 treatment in N2a cells (Fig. 4a–c). We also used two PIK3C3 complex inhibitors 3-MA and SAR405 to inhibit the lipidation of LC3B [33]. Following CB6 treatment, LC3B-II levels were induced in control cells, whereas 3-MA and SAR405 suppressed the induction of LC3B-II levels (Fig. 4d–i). On the other hand, treatment of 3-MA or SAR405 rescued the loss of SQSTM1 protein in CB6-treated cells (Fig. 4d–i). To further confirm these results, we transfected N2a cells with GFP-LC3 plasmids to observe the LC3 puncta formation. The number of LC3 puncta was significantly increased by CB6 treatment alone but was blocked by the cotreatment of SAR405, indicating that SAR405 inhibited CB6-induced lipidation of LC3 (Fig. 4j, k). In other words, CB6-induced autophagy is dependent on the PIK3C3 complex.

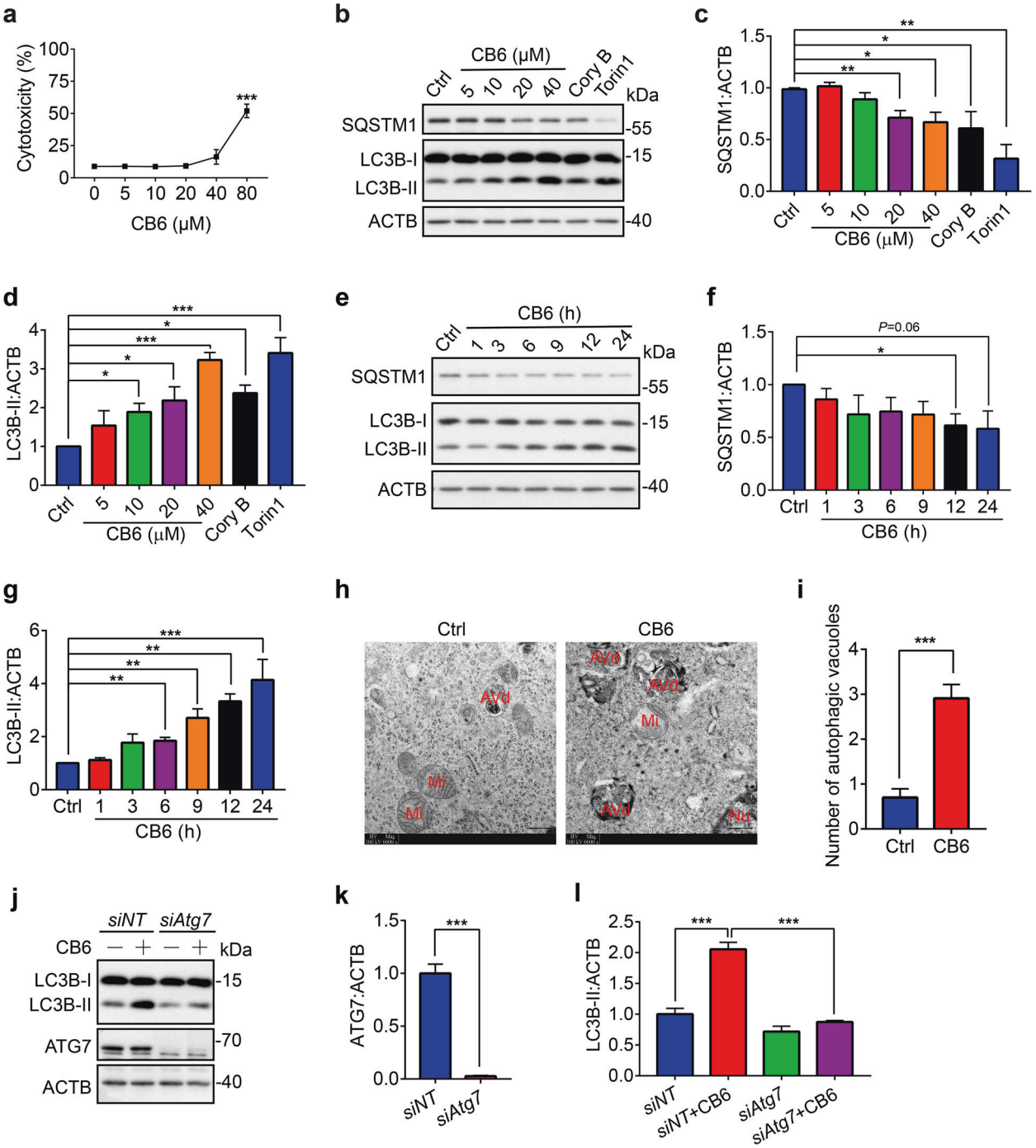


**Fig. 1 CB6 induces autophagy in neural cells. a** N2a cells were treated with the indicated concentration of CB6 for 24 h and then the cytotoxicity was detected by LDH assays. **b** Representative Western blots show the levels of autophagy markers (SQSTM1/P62 and LC3B) in N2a cells. N2a cells were treated with different concentrations of CB6 for 12 h. Cory B (20 μM) and Torin 1 (250 nM) were used as positive controls. **c**, **d** The relative levels of SQSTM1 and LC3B-II in **b** were quantified as mean ± SEM from three independent experiments. $^{*}P < 0.05$, $^{**}P < 0.01$ and $^{***}P < 0.001$ vs. Ctrl group. **e** Representative Western blots show the levels of SQSTM1 and LC3B in N2a cells. N2a cells were treated with CB6 (20 μM) for indicated durations. **f**, **g** The relative levels of SQSTM1 and LC3B-II in **e** were quantified as mean ± SEM from three independent experiments. $^{*}P < 0.05$, $^{**}P < 0.01$ and $^{***}P < 0.001$ vs. Ctrl group. **h** Representative transmission electron microscopic images show autophagic compartments in N2a cells. N2a cells were treated with DMSO or CB6 (20 μM) for 14 h, fixed with 2.5% glutaraldehyde for 1 h. Mi, mitochondria; AVd, degradative autophagic vacuole; Nu, nucleus. Scale bar: 500 nm. **i** Statistical results for the number of autophagic compartments in each image. At least 20 images were analyzed in each group. $^{***}P < 0.001$ vs. Ctrl group. **j** Representative Western blots show the levels of LC3B in N2a cells. N2a cells were transfected with nontarget (*NT*) or *Atg7* specific siRNA for 60 h and then treated with CB6 (20 μM) for 12 h. **k** The relative levels of ATG7 in **j** were quantified as mean ± SEM from three independent experiments. $^{***}P < 0.001$ vs. *siNT* group. **i** The relative levels of LC3B-II in **k** were quantified as mean ± SEM from three independent experiments. $^{***}P < 0.001$ vs. *siNT* + CB6 group.

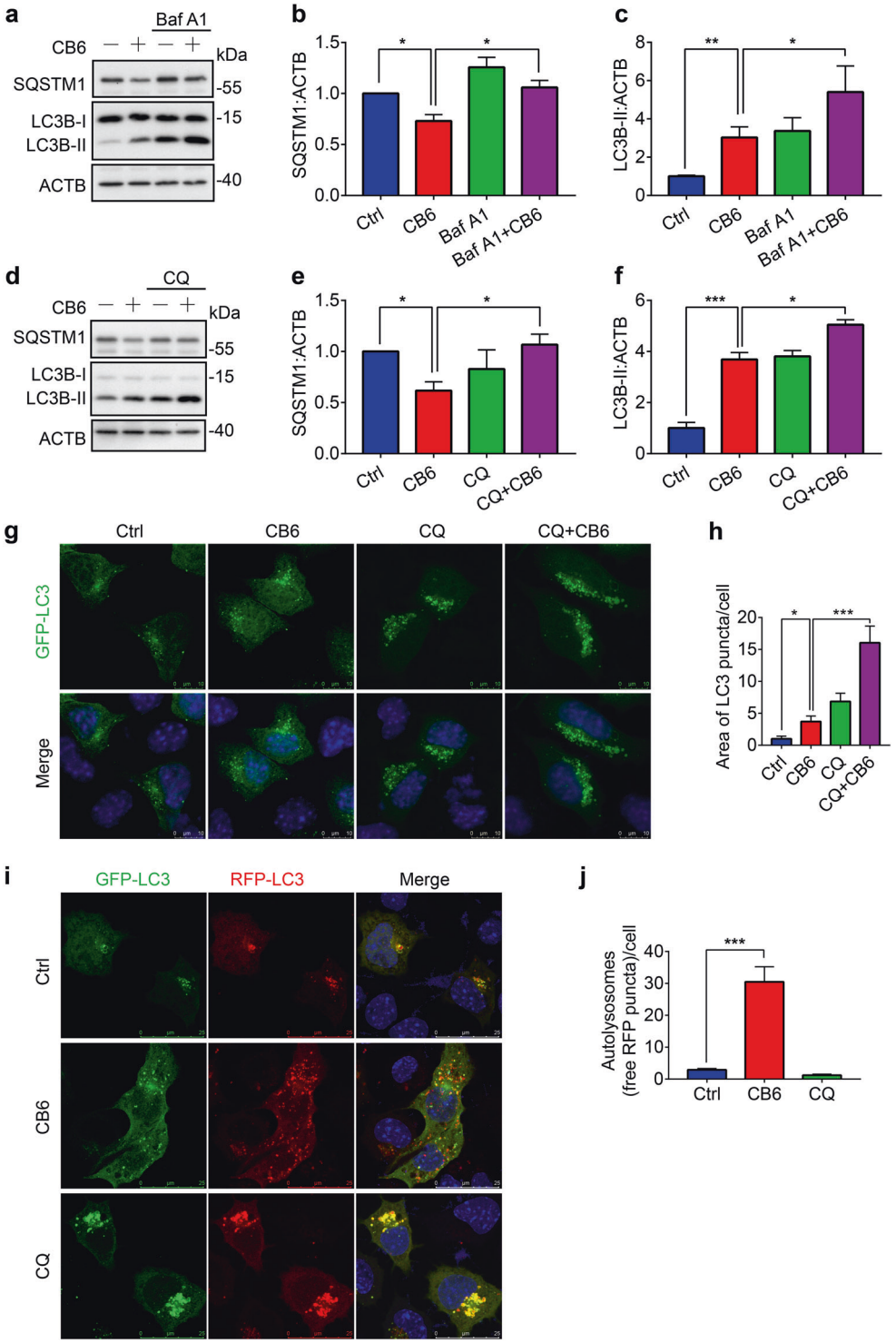


**Fig. 2 CB6 induces autophagy flux in neural cells. a** Representative Western blots show the levels of SQSTM1 and LC3B in N2a cells. N2a cells were treated with CB6 (20 μM) for 12 h. Three hours before harvesting cells, the v-ATPase inhibitor bafilomycin A1 (Baf A1, 100 nM) was added to the cell culture medium to inhibit the autophagosome-lysosome fusion. **b**, **c** The relative levels of SQSTM1 and LC3B-II in **a** were quantified as mean ± SEM from three independent experiments. $^{*}P < 0.05$ and $^{**}P < 0.01$ vs. CB6 group. **d** Representative Western blots show the levels of SQSTM1 and LC3B in N2a cells. N2a cells were treated with CB6 (20 μM) for 12 h. Three hours before harvesting cells, the lysosomal inhibitor chloroquine (CQ, 100 μM) was added into cells to block the lysosomal degradation. **e**, **f** The relative levels of SQSTM1 and LC3B-II in **d** were quantified as mean ± SEM from three independent experiments. $^{*}P < 0.05$ and $^{***}P < 0.001$ vs. CB6 group. **g** Representative immunostaining images show the pattern of GFP-LC3 in N2a cells. N2a cells were transfected with GFP-LC3 plasmids for 24 h and then treated with CB6 (20 μM) for 12 h with or without CQ (100 μM) (CQ was added into cells 3 h before fixing cells). Scale bar: 10 μm. **h** Statistical results for the area of green puncta in each cell in **g**. At least 25 cells were analyzed in each group. $^{*}P < 0.05$ and $^{***}P < 0.001$ vs. CB6 group. **i** Representative immunostaining images show the pattern of tf-LC3 in N2a cells. N2a cells were transfected with tf-LC3 plasmids for 24 h and then treated with CB6 (20 μM) for 12 h using CQ (100 μM) as a negative control. Scale bar: 25 μm. **j** Statistical results for the mean number of autolysosomes (puncta with red color in merged images) in each cell in (**i**). Data were quantified as mean ± SEM. $^{***}P < 0.001$ vs. Ctrl group.

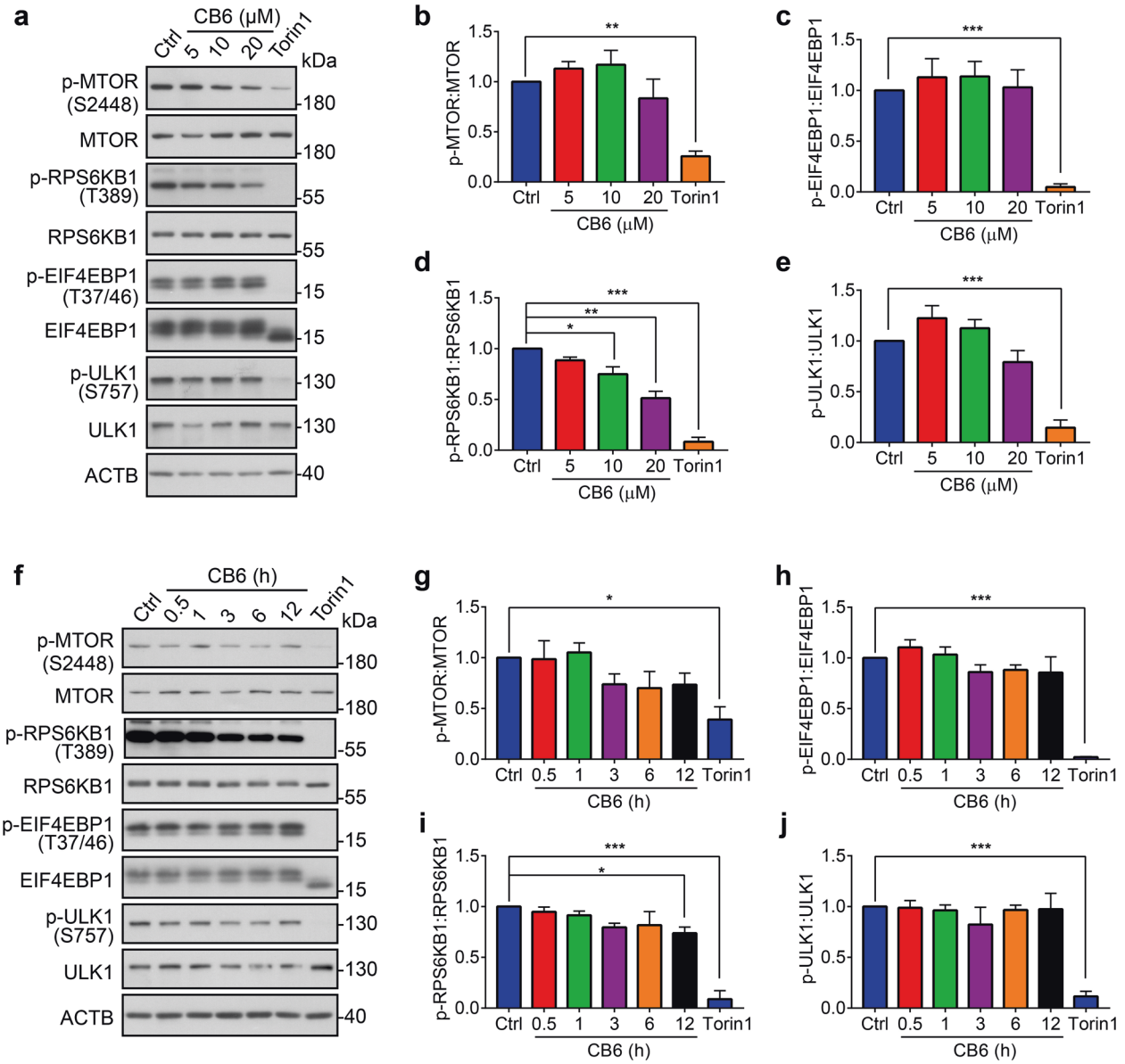


**Fig. 3 CB6-induced autophagy is independent of the MTORC1 pathway.** Representative Western blots show the levels of total and phosphorylated MTOR, EIF4EBP1, RPS6KB1, and ULK1 in N2a cells. **a** N2a cells were treated with different concentrations of CB6 for 12 h using Torin 1 (250 nM) as a positive control. The relative levels of p-MTOR (**b**), p-EIF4EBP1 (**c**), p-RPS6KB1 (**d**), and p-ULK1 (**e**) in (**a**) were quantified as mean ± SEM from three independent experiments. *$P < 0.05$, **$P < 0.01$ and ***$P < 0.001$ vs. Ctrl group. **f** N2a cells were treated with CB6 (20 μM) for the indicated durations. The relative levels of p-MTOR (**g**), p-EIF4EBP1 (**h**), p-RPS6KB1 (**i**), and p-ULK1 (**j**) in (**f**) were quantified as mean ± SEM from three independent experiments. *$P < 0.05$ and ***$P < 0.001$ vs. Ctrl group.

Since the PIK3C3 complex is involved in CB6-induced autophagy, we tried to identify whether CB6 increases the activity of the PIK3C3 complex. This complex is primarily responsible for the production of PI3P, which is required for the formation of the phagophore and can be detected by the proteins containing FYVE, PX, or WD40 domains [31, 34]. Immunofluorescence assay showed that CB6 treatment increased the number of GFP-FYVE (PI3P probe) puncta in N2a cells, indicating CB6 activated the PIK3C3 complex and promoted the production of PI3P (Fig. 5a, b). This increase could be blocked by PIK3C3 inhibitor SAR405, suggesting that CB6 enhanced PI3P production through activating the PIK3C3 complex (Fig. 5a, b). Moreover, to evaluate the activity of the PIK3C3 complex directly, endogenous PIK3C3 complex was immunoprecipitated from the N2a cell lysates with or without CB6 treatment. Then the enzyme activity of the PIK3C3 complex was determined by using an ELISA kit. The ELISA results showed that CB6 treatment effectively promoted the production of PI3P, suggesting CB6 enhances the activity of the PIK3C3 complex (Fig. 5c).

Then we determined whether CB6 enhances the activity of the PIK3C3 complex by regulating the assembly or disassembly of its core components including PIK3R4, PIK3C3, ATG14, UVRAG, RUBCN, BECN1, and BCL2 [35–37]. N2a cells were treated with or without CB6, and the PIK3C3 complex was immunoprecipitated by using anti-PIK3C3 or anti-BECN1 antibodies. We found that CB6 treatment did not change the levels of the immunoprecipitated interacting proteins, indicating that CB6 does not affect the assembly of the PIK3C3 complex (Supplementary Fig. S4a, b). Similar results were also confirmed in HEK 293 cells (Supplementary Fig. S4c). Furthermore, we used exogenous Flag-BECN1 or Flag-ATG14 to immunoprecipitate the PIK3C3 complex and found that CB6 did not alter the assembly of main components of the

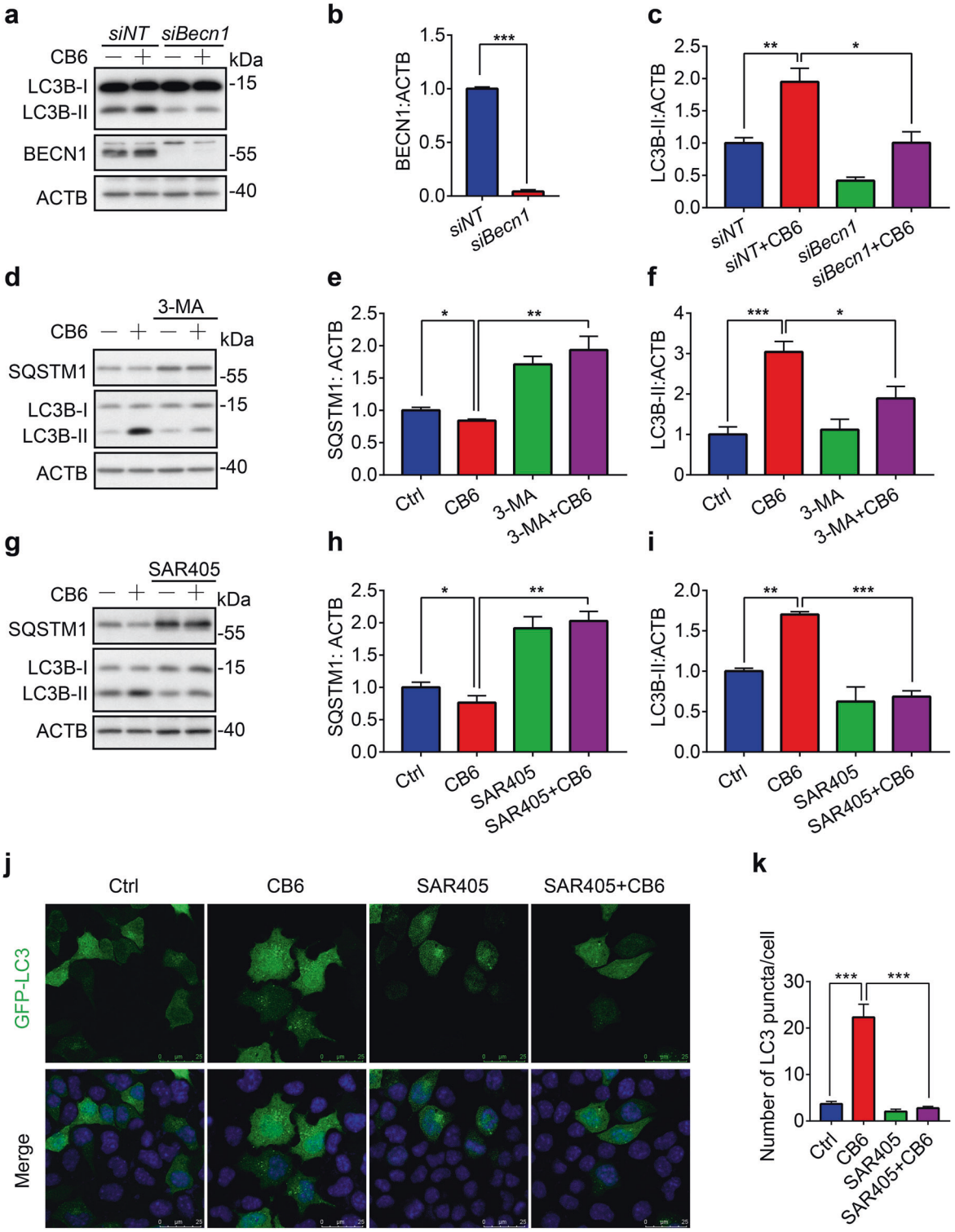


**Fig. 4 PIK3C3 complex is involved in CB6-induced autophagy. a** After transfection with nontarget or *Becn1* specific siRNAs for 60 h, N2a cells were treated with CB6 (20 μM) for another 12 h. **b** The relative levels of BECN1 in (**a**) were quantified as mean ± SEM from three independent experiments. ***$P < 0.001$ vs. *siNT* group. **c** The relative levels of LC3B-II in (**a**) were quantified as mean ± SEM from three independent experiments. *$P < 0.05$ and **$P < 0.01$ vs. *siNT* + CB6 group. **d** After pretreatment with PIK3C3 inhibitor 3-methyladenine (3-MA, 5 mM) for 30 min, N2a cells were treated with CB6 (20 μM) for another 12 h. **e**, **f** The relative levels of SQSTM1 and LC3B-II in **d** were quantified as mean ± SEM from three independent experiments. *$P < 0.05$, **$P < 0.01$ and ***$P < 0.001$ vs. CB6 group. **g** After pretreatment with PIK3C3 inhibitor SAR405 (5 μM) for 30 min, N2a cells were treated with CB6 (20 μM) for 12 h. **h**, **i** The relative levels of SQSTM1 and LC3B-II in **g** were quantified as mean ± SEM from three independent experiments. *$P < 0.05$, **$P < 0.01$ and ***$P < 0.001$ vs. CB6 group. (**j**) Representative immunostaining images show the pattern of GFP-LC3 in N2a cells. After transfection with GFP-LC3 plasmids for 24 h, N2a cells were treated with CB6 (20 μM) for 12 h in the presence or absence of SAR405 (5 μM) (SAR405 was added into cells 30 min before CB6 treatment). Scale bar: 25 μm. **k** Statistical results for the mean number of green puncta in each cell in **j**. At least 20 cells were analyzed in each group. ***$P < 0.001$ vs. CB6 group.

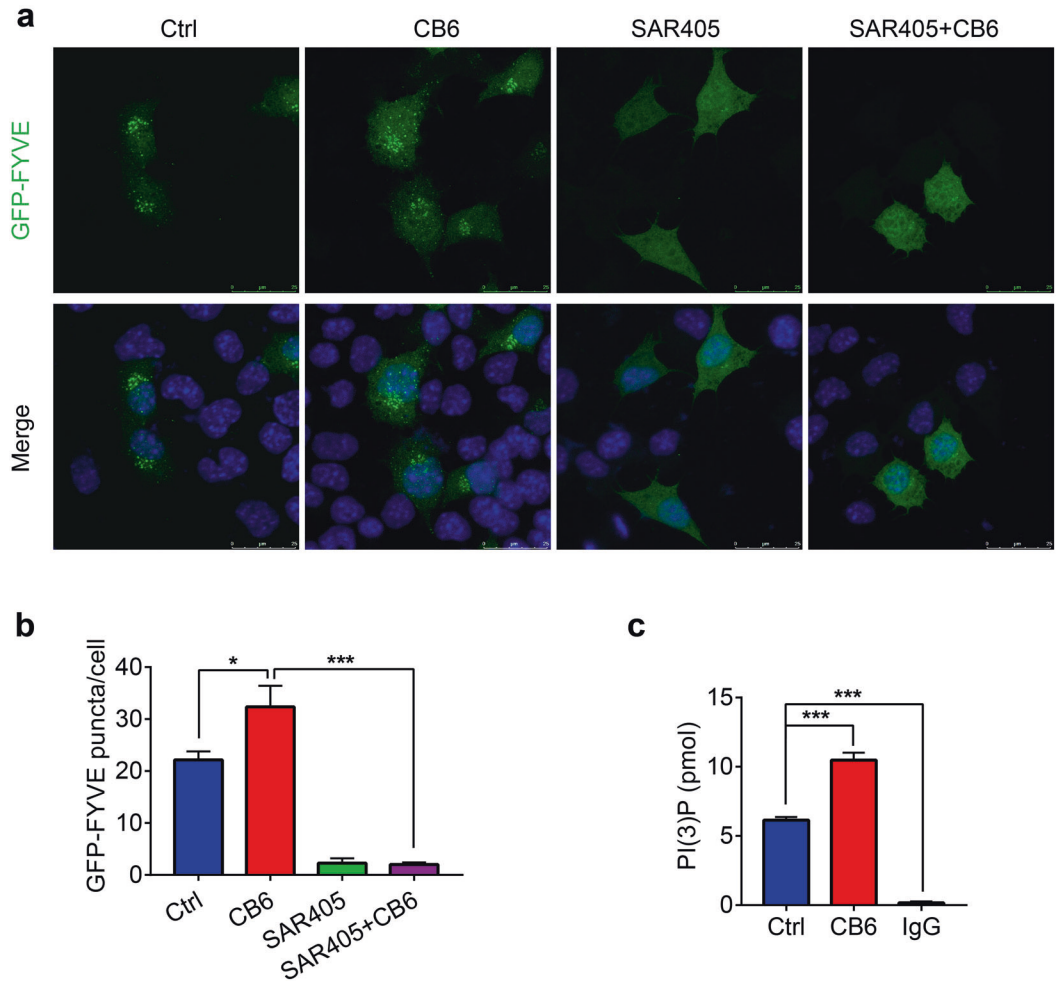


**Fig. 5 CB6 enhances the activity of the PIK3C3 complex. a** Representative immunostaining images show the pattern of GFP-FYVE (a PI3P binding reporter) in N2a cells. After transfection with GFP-FYVE plasmids for 24 h, N2a cells were treated with SAR405 (5 μM) and CB6 (20 μM) for 12 h (SAR405 was added into cells 30 min before CB6 treatment). **b** Statistical results for the mean number of GFP-FYVE puncta in each cell. At least 15 cells were analyzed in each group. $^{*}P < 0.05$ and $^{***}P < 0.001$ vs. Ctrl group. **c** Representative ELISA assay shows the amount of PI3P produced in each group. After N2a cells were treated with CB6 (20 μM) for 6 h, PIK3C3 complex was immunoprecipitated from cell lysates using BECN1 antibody-coated magnetic beads, followed by kinase reaction. The quantification of the product PI3P was determined by PIK3C3 Kit. $^{***}P < 0.001$ vs. Ctrl group.

PIK3C3 complex in HEK 293 cells (Supplementary Fig. S4d). Together, these results indicate that CB6 enhances the activity of the PIK3C3 complex without affecting the assembly of the PIK3C3 complex.

### PIK3C3-dependent autophagy is involved in CB6's neuroprotective effects in an $MPP^+$-induced cellular model of PD

Because CB6 is brain permeable and because it induces MTORC1-independent autophagy in neural cells, we hypothesized that CB6 may be a promising drug candidate for the treatment of PD. We used PC12 cells as a model of dopaminergic neurons to establish a cellular model of PD induced by $MPP^+$. This cellular model has been widely used for in vitro studies as $MPP^+$ is the active metabolite of neurotoxin MPTP, which selectively causes the degeneration of nigrostriatal dopaminergic neurons in PD [38, 39].

To establish a cellular model of PD, PC12 cells were treated with different concentrations of $MPP^+$ for 48 h and then the cell viability was measured by the alamarBlue assay. The cell viability was significantly decreased by the treatment of $MPP^+$ in a dose-dependent manner (Fig. 6a). $MPP^+$ (1 mM) was selected for the following experiments. To investigate the neuroprotective effects of CB6 in the cellular model of PD, PC12 cells were pretreated with different concentrations of CB6 for 0.5 h and then cotreated with $MPP^+$ for another 48 h. As expected, the cell viability was increased by 46% upon CB6 treatment in the cellular model of PD (Fig. 6b). However, CB6's protective effects were abolished by a lysosome inhibitor CQ, indicating the neuroprotective effects of CB6 involve autophagic and lysosomal degradation (Fig. 6c). As CB6-induced autophagy requires the PIK3C3 complex, we then examined whether the PIK3C3 complex is involved in the neuroprotective effects of CB6. We noted that PIK3C3 complex inhibitor SAR405 blocked the neuroprotective effects of CB6, as shown in the cell viability results (Fig. 6d). Similar results were also confirmed by another PIK3C3 complex inhibitor Spautin1 (Fig. 6e). Moreover, the neuroprotective effects of CB6 were also abolished by knocking down *Becn1* in PC12 cells (Fig. 6f). The results indicate that PIK3C3-dependent autophagy is involved in the neuroprotective effects of CB6 in the $MPP^+$-induced cellular model of PD.

### CB6 induces autophagy and inhibits apoptosis in an $MPP^+$-induced cellular model of PD

The inhibition of autophagy is reportedly involved in the cytotoxicity of $MPP^+$ in the cellular model of PD [40]. To verify whether CB6 induces autophagy in an $MPP^+$-induced cellular model of PD, we detected an autophagy substrate SQSTM1 in PC12 cells. First, in immunofluorescence experiments, SQSTM1 showed a pattern of

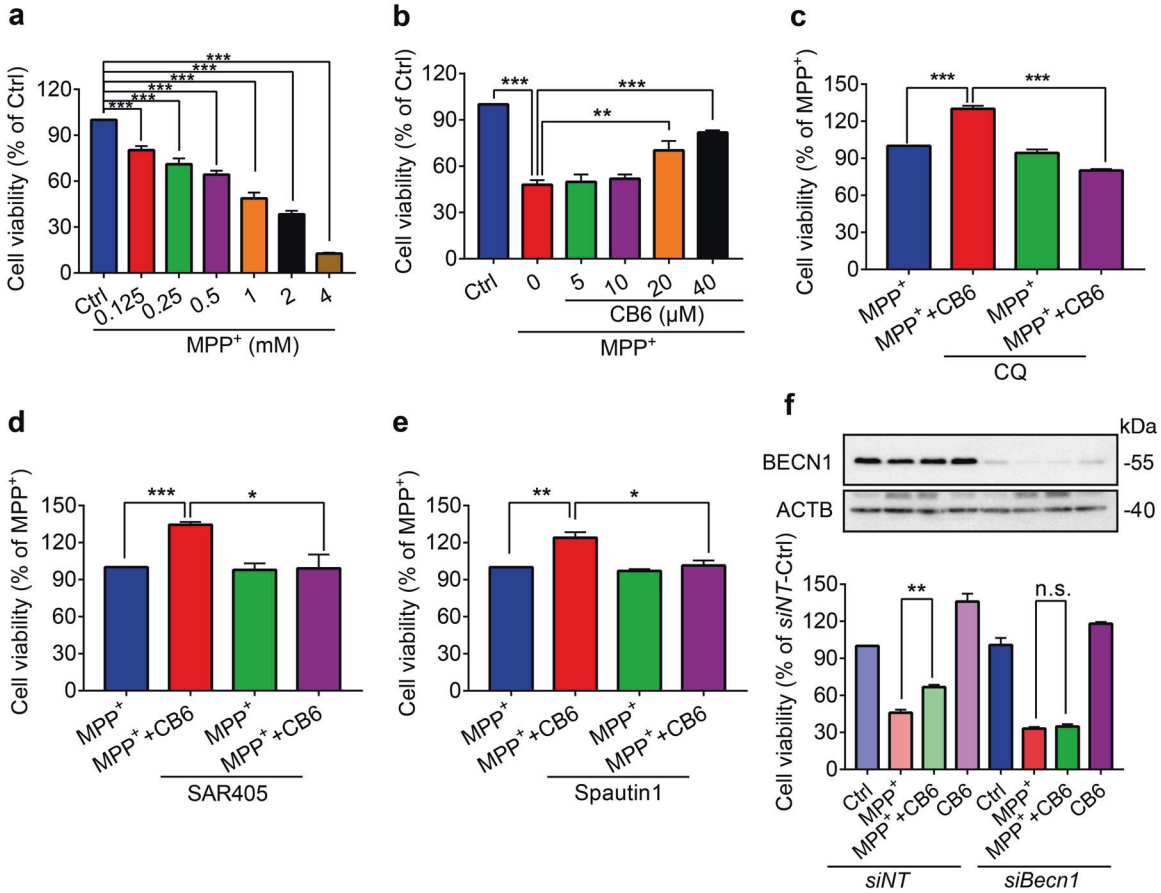


**Fig. 6 PIK3C3 complex-dependent autophagy is involved in the neuroprotective effects of CB6 in MPP$^+$-treated PC12 cells. a** PC12 cells were treated with different concentrations of MPP$^+$ for 48 h and then the cell viability was measured using alamarBlue assay. Data were quantified as mean ± SEM from three independent experiments. ***$P < 0.001$ vs. Ctrl group. **b** PC12 cells were pretreated with different concentrations of CB6 for 30 min, followed by cotreatment with MPP$^+$ (1 mM) for another 48 h. Data were quantified as mean ± SEM from three independent experiments. **$P < 0.01$ and ***$P < 0.001$ vs. MPP$^+$ group. **c** After treatment of CB6 (20 μM) and CQ (50 μM) for 30 min, PC12 cells were treated with MPP$^+$ (1 mM) for another 48 h. Data were quantified as mean ± SEM from three independent experiments. ***$P < 0.001$ vs. MPP$^+$ + CB6 group. After treatment of CB6 (20 μM) and SAR405 (5 μM) (**d**) or Spautin1 (10 μM) (**e**) for 30 min, PC12 cells were treated with MPP$^+$ (1 mM) for another 48 h. Data were quantified as mean ± SEM from three independent experiments. *$P < 0.05$, **$P < 0.01$ and ***$P < 0.001$ vs. MP$P^+$ + CB6 group. (**f**) PC12 cells were transfected with nontarget or *Becn1* specific siRNA for 24 h, followed by co-treatment with CB6 (20 μM) and MPP$^+$ (1 mM) for another 48 h. Data were quantified as mean ± SEM from three independent experiments. **$P < 0.01$ vs. *siNT* + MPP$^+$ group. n.s., not significant. Western blots show the knockdown efficacy of *Becn1* in PC12 cells.

dispersed small puncta in both CB6-treated cells and control cells (Fig. 7a). However, it turned into a pattern of inhomogeneous large puncta in MPP$^+$-treated cells, indicating the formation of SQSTM1 aggregates. However, this pattern was rescued by CB6 pretreatment, suggesting CB6 prevented SQSTM1 aggregation, which was induced by MPP$^+$ treatment (Fig. 7a). CQ was used as a negative control, showing a similar pattern as MPP$^+$-treated cells (Fig. 7a). We next applied Western blot analysis to examine the protein levels in Triton X-100-soluble and -insoluble fractions of cell lysates. Considering protein levels are regulated by synthesis and degradation rates, we used CHX (5 μg/mL, 14 h) to block the protein synthesis of SQSTM1, and only the degradation rate of SQSTM1 was detected. After CHX treatment, SQSTM1 protein levels were dramatically decreased in the Triton X-100-soluble fractions, indicating CHX successfully blocked the synthesis of SQSTM1 (Fig. 7b). Compared with the control cells in the presence of CHX, we found that MPP$^+$ treatment significantly decreased LC3B-II levels in the soluble fractions but increased SQSTM1 levels in the insoluble fractions, indicating MPP$^+$ inhibits autophagy in PC12 cells (Fig. 7b, c). In the Triton X-100-insoluble fractions, CB6 treatment statistically decreased SQSTM1 levels in MPP$^+$-treated cells (Fig. 7b, c). These data indicate that CB6 promotes the degradation of insoluble SQSTM1 in the cellular model of PD. To demonstrate whether CB6-induced degradation of insoluble SQSTM1 was through activating autophagy, we cotreated PC12 cells with CQ to block autophagic degradation. In the cellular model of PD, CB6-induced downregulation of the insoluble SQSTM1 levels was significantly blocked by CQ treatment (Fig. 7b, c). Similar results were also confirmed by another autophagy substrate ubiquitinated-protein aggregates (Fig. 7b, d). Overall, these results indicate that CB6 induces autophagy and enhances autophagic degradation in MPP$^+$-treated PC12 cells.

Because MPP$^+$ induces neural cell death by activating CASP3-dependent apoptosis [41] and because mounting evidence has shown induction of autophagy has been a potential strategy to prevent apoptosis [42], we hypothesized that the neuroprotective effects of CB6 are through inducing autophagy and thereby inhibiting MPP$^+$-induced apoptosis. In the presence of CHX, MPP$^+$ treatment markedly increased protein levels of cleaved PARP1 and cleaved CASP3 (apoptosis markers) in PC12 cells (Fig. 7e–g). Conversely, CB6 treatment drastically abolished the MPP$^+$-increased levels of cleaved PARP1 and cleaved CASP3 (Fig. 7e–g).

The CB6's anti-apoptotic effects were further blocked by CQ cotreatment (Fig. 7e–g). Similarly, ActD (0.1 μM, 24 h) was also used to inhibit RNA synthesis, and the anti-apoptotic effects of

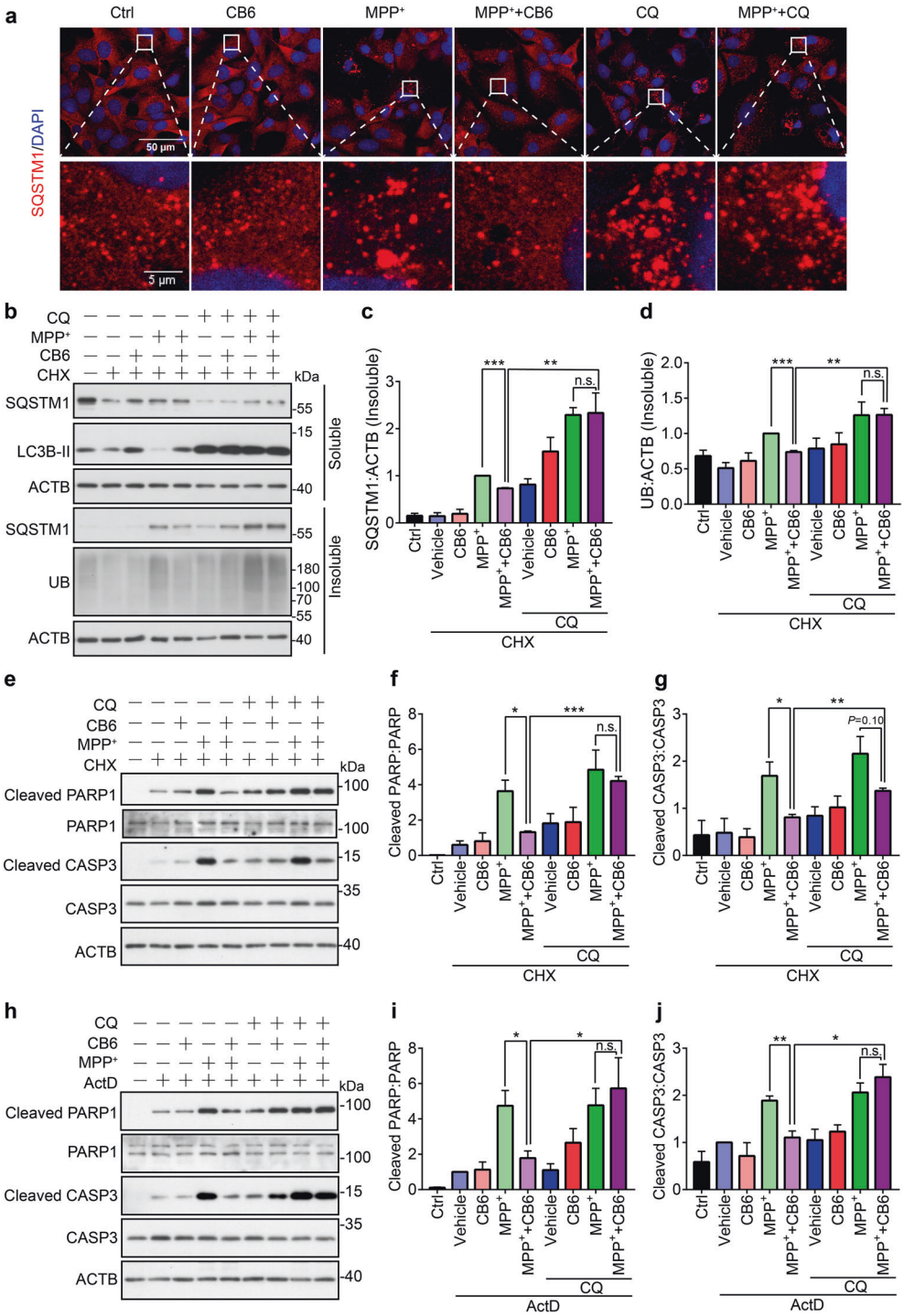


**Fig. 7 CB6 induces autophagy and inhibits apoptosis in MPP$^+$-treated PC12 cells. a** Representative immunostaining images show the pattern of SQSTM1 in PC12 cells. PC12 cells were pretreated with CB6 (20 μM) for 30 min, followed by cotreatment with MPP$^+$ (1 mM) for another 48 h, and then the cells were fixed for immunostaining. PC12 cells were treated with CQ (50 μM) for 24 h. **b** PC12 cells were pretreated with CB6 (20 μM), followed by cotreatment with MPP$^+$ (1 mM) for another 48 h with or without protein synthesis inhibitor cycloheximide (CHX, 5 μg/mL) (CHX was added into cells 14 h before cell harvesting). PC12 cells were treated with CQ (50 μM) for 24 h. The cell lysates were separated into the Triton X-100-soluble and -insoluble fractions. The levels of autophagy markers (SQSTM1, UB/Ubiquitin, and LC3B) were detected by Western blot analysis. The relative levels of SQSTM1 (**c**) and UB (**d**) in the insoluble fractions were quantified as mean ± SEM from three independent experiments. $^{**}P < 0.01$ and $^{***}P < 0.001$ vs. CHX + MPP$^+$ + CB6 group. **e** After treatment with CB6 (20 μM) for 30 min, PC12 cells were treated with MPP$^+$ (1 mM) for another 48 h. CHX (5 μg/mL) was added into cells 14 h before cell harvesting. The levels of apoptosis-related protein (total and cleaved PARP1 and CASP3) were detected by Western blot analysis. The relative levels of cleaved PARP1 (**f**) and cleaved CASP3 (**g**) were quantified as mean ± SEM from three independent experiments. $^{*}P < 0.05$, $^{**}P < 0.01$ and $^{***}P < 0.001$ vs. CHX + MPP$^+$ + CB6 group. **h** After treatment with CB6 (20 μM) for 30 min, PC12 cells were cotreated with MPP$^+$ (1 mM) for another 48 h. An mRNA synthesis inhibitor actinomycin D (ActD, 0.1 μM) was added to cells 24 h before cell harvesting. Total and cleaved PARP1 and CASP3 were detected by Western blot analysis. The relative levels of cleaved PARP1 (**i**) and cleaved CASP3 (**j**) were quantified as mean ± SEM from three independent experiments. $^{*}P < 0.05$ and $^{**}P < 0.01$ vs. CHX + MPP$^+$ + CB6 group.

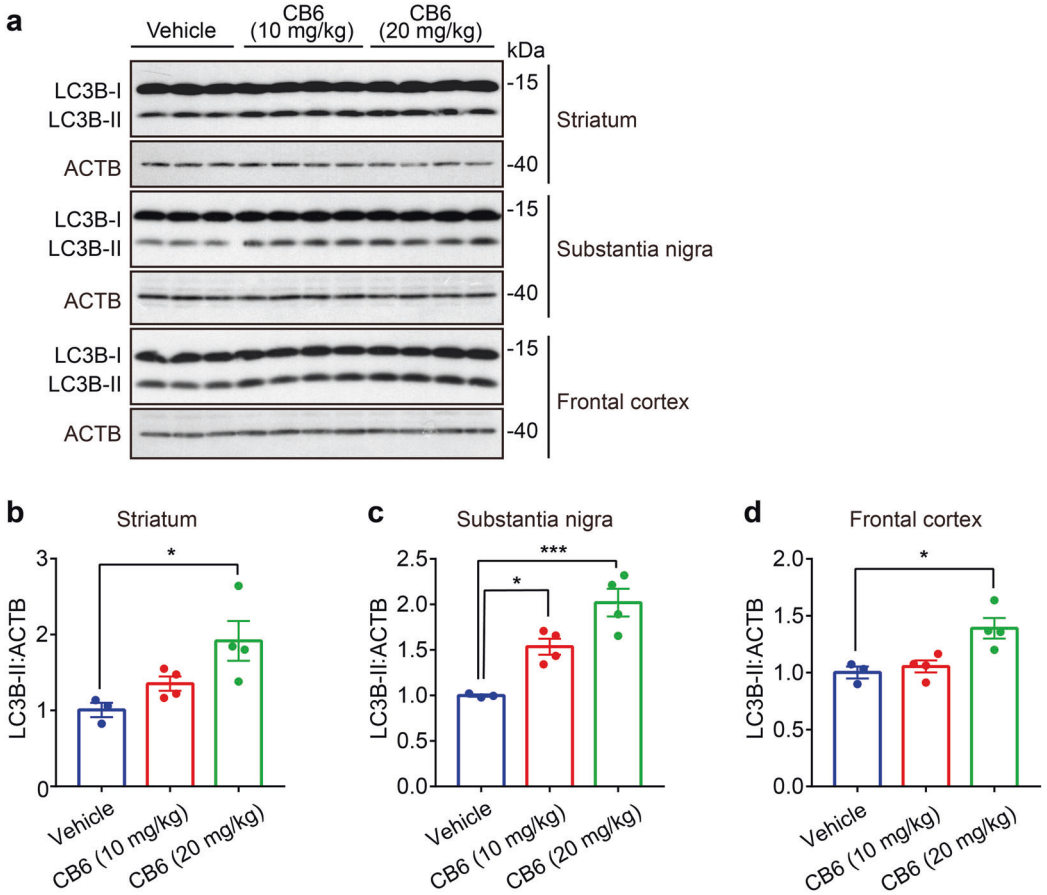


**Fig. 8 CB6 induces autophagy marker (LC3B-II levels) in mouse brains.** After oral administration with 10 mg/kg or 20 mg/kg CB6 for one week, mice were sacrificed. Different regions (striatum, substantia nigra, and frontal cortex) of brains were dissected for processing. **a** Expression levels of LC3B in different regions of mouse brains were examined by Western blot analysis. Relative levels of LC3B-II in striatum (**b**), substantia nigra (**c**) and frontal cortex (**d**) were quantified as mean ± SEM (male, $n = 3$ or 4). $^{*}P < 0.05$ and $^{***}P < 0.001$ vs. Vehicle group

CB6 in $MPP^{+}$-treated PC12 cells were analyzed subsequently. In the presence of ActD, $MPP^{+}$ increased the protein levels of cleaved PARP1 and cleaved CASP3, which were rescued by CB6 treatment (Fig. 7h–j). Furthermore, CQ treatment blocked the anti-apoptotic effects of CB6 in the presence of ActD (Fig. 7h–j). Collectively, these results imply that CB6 exerts anti-apoptotic and neuroprotective roles in $MPP^{+}$-treated PC12 cells by inducing autophagy.

## CB6 protects dopaminergic neurons in an MPTP mouse model of PD

Because CB6 has good brain permeability (Supplementary Fig. S1) and because it protects neural cells from $MPP^{+}$-induced apoptosis by enhancing autophagy (Fig. 7), we hypothesized that CB6 would also exert neuroprotective effects in mouse models of PD through inducing autophagy. Firstly, to demonstrate CB6 was able to induce autophagy in mouse brains, C57BL/6 mice were orally administered 10 mg/kg or 20 mg/kg CB6 for one week. Different regions (striatum, substantia nigra, and frontal cortex) of the brains were dissected and further processed for Western blot analysis. CB6 treatment increased LC3B-II levels in these three regions of brains, indicating that CB6 treatment induced autophagy in mouse brains (Fig. 8a–d). We then used an MPTP mouse model of PD to test the neuroprotective effects of CB6 in vivo [43]. A timeline of mice experiments was shown in Fig. 9a. After MPTP injection, mouse weights decreased slightly but recovered later (Fig. 9b). For the behavioral experiments, rotarod was used to evaluate mice's motor coordination. The latency to fall was slightly decreased in MPTP-treated mice compared to saline-treated mice (Fig. 9c). However, CB6 treatment significantly increased the latency to fall in MPTP-treated mice (Fig. 9c). These results indicate that CB6 treatment ameliorates motor impairment induced by MPTP in C57BL/6 mice.

After confirming the motor ability-enhancing effects of CB6 in MPTP-treated mice, we used a TH antibody to stain dopaminergic neurons in the striatum and substantia nigra pars compacta (SNpc) of brains. For the MPTP group, the density of TH dramatically decreased in the striatum, which was consistent with a decrease in the motor ability of mice injected with MPTP (Fig. 10a, b). In contrast, CB6 treatment markedly increased the density of TH in the striatum, compared with the MPTP group (Fig. 10a, b). In addition, the number of TH-positive dopaminergic neurons in the SNpc was decreased in the MPTP group, whereas this decrease was rescued in the MPTP + CB6 groups (Fig. 10c, d). The content of TH in mouse brains was also confirmed by Western blot analysis. TH protein levels were drastically decreased in the MPTP group, but this decrease was abolished by CB6 administration (Fig. 10e, f). These results indicated that CB6 treatment rescued the decreased number of dopaminergic neurons in the MPTP-treated mouse model of PD. To further confirm the neuroprotective effects of CB6, we used LC-MS/MS assay to detect striatal dopamine and its metabolites DOPAC and HVA levels, which are markers of dopaminergic synaptic function. Comparing the MPTP group with the saline group, the concentrations of striatal dopamine, DOPAC, and HVA were markedly decreased by 75%, 78%, and 64% respectively (Fig. 10g–i).

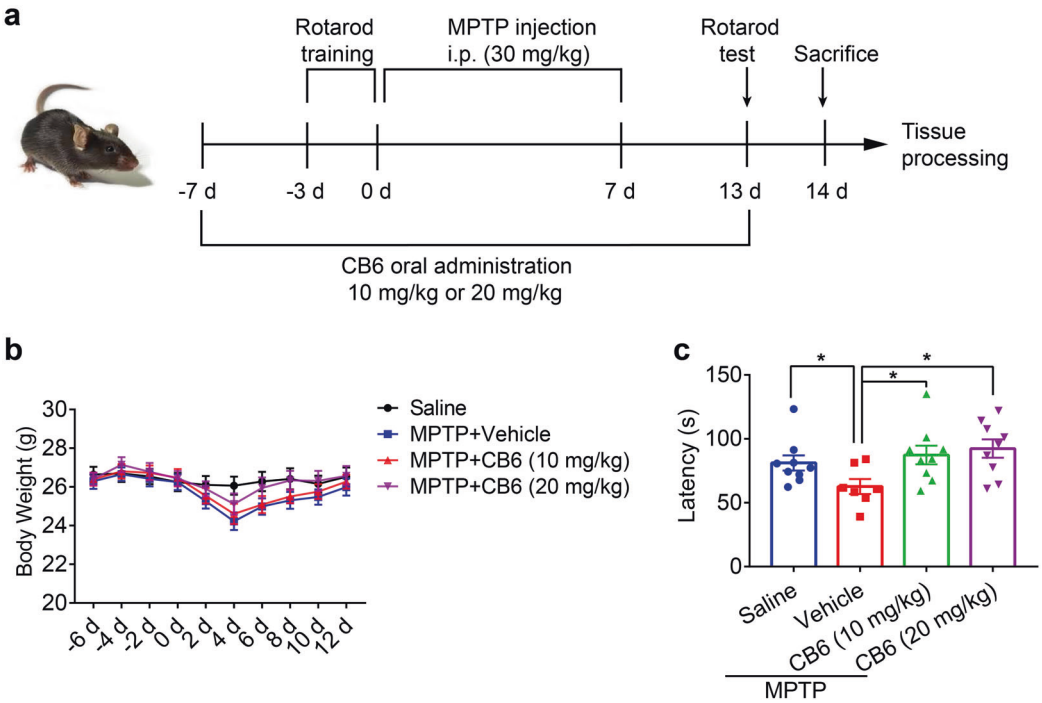


**Fig. 9 CB6 treatment on an MPTP mouse model of Parkinson's disease (PD). a** Drug treatment and behavioral study scheme with C57BL/6 mice. MPTP was injected intraperitoneally (i.p.) for 7 consecutive days. CB6 was orally administered for 21 consecutive days and the first administration was 7 days before MPTP first injection. After all treatment, the mice were subjected to behavioral tests. **b** Mice weights were measured every two days. **c** Rotarod was chosen for mice behavioral tests and the latency to fall was recorded. Data were quantified as mean ± SEM ($n = 7–9$). *$P < 0.05$ vs. MPTP group.

However, CB6 administration rescued the decrease in striatal dopamine, DOPAC, and HVA levels, especially in the mice given high doses of CB6 (20 mg/kg) (Fig. 10g–i). In summary, CB6 has neuroprotective effects on dopaminergic neurons in the MPTP mouse model of PD.

## DISCUSSION

Accumulating evidence has suggested that restoration of autophagy flux to degrade pathological proteins is a potential method to develop new drug candidates to treat neurodegenerative diseases, including PD [6, 16]. Our previous study demonstrated that a natural alkaloid Cory B can induce autophagy and promote SNCA degradation in vitro [20]. However, the underlying mechanisms were not fully understood, and the brain permeability of Cory B was relatively low, which limits its potential use in treating neurodegenerative diseases. To improve the brain bioavailability and potency of Cory B for treating PD, a Cory B derivate termed CB6 was synthesized. CB6 passes through the BBB more quickly and easily, and its efficient concentration in brains is much higher than Cory B. In this study, we systematically investigated the autophagy-inducing effects of compound CB6. We demonstrated that CB6 enhanced the activity of the PIK3C3 complex to promote PI3P production, thus accelerating autophagy flux (Fig. 11). Since neurotoxin $MPP^+$ activates CASP3-dependent apoptosis and autophagy enhancers are emerging as apoptosis inhibitors [41, 42], autophagy enhancers are promising to exert neuroprotective effects against $MPP^+$-induced cytotoxicity. In the $MPP^+$-induced cellular model of PD, we demonstrated that CB6 inhibited neural cell apoptosis and increased cell viability by inducing autophagy (Fig. 11). The in vivo studies further proved that CB6 prevents the loss of dopaminergic neurons in an MPTP mouse model of PD. However, it warrants further studies about how CB6 upregulates the activity of the PIK3C3 complex in vitro and whether the neuroprotective effects of CB6 are through PIK3C3 complex-mediated autophagy in vivo.

We previously reported that Cory B has autophagy-inducing effects in a cellular model of PD. It induces MTORC1-independent autophagy in a BECN1-dependent manner, thus promoting SNCA degradation in SNCA-overexpressed N2a cells [20]. Cory B also interrupts the interaction of SNCA and HMGB1 to restore autophagy in PC12 cells [22]. It also has been reported that Cory B is neuroprotective in manganese-exposed SH-SY5Y cells through inducing HMGB1-dependent autophagy [44]. However, all the reports about Cory B were studied in cellular models of PD. Due to its limited brain permeability, the neuroprotective effects of Cory B in an MPTP mouse model of PD have not been studied. In this study, to improve the bioavailability of Cory B in animal models, CB6 was synthesized to have better brain permeability (Supplementary Fig. S1), which is beneficial for the candidate drugs to treat neurodegenerative diseases. Brain permeability studies showed that, compared with Cory B, the peak concentration of CB6 in brains was higher and a larger proportion of CB6 passed through the BBB. Ideally, this results in fewer side effects of CB6. Moreover, brain-permeable CB6 showed neuroprotective properties in vivo, like successfully restoring motor dysfunction and preventing the dopaminergic neuron loss in the MPTP mouse model of PD (Figs. 9, 10).

Previously, we reported that Cory B induced BECN1-dependent but MTORC1-independent autophagy at the dose of 25 μM [20]. However, other studies reported 50 μM or above of Cory B inhibited MTORC1 signaling [44]. In this study, since CB6 was synthesized from Cory B, it may have similar effects on MTORC1 pathway. We found that 12-h treatment of 20 μM CB6 inhibits the MTORC1 pathway in N2a cells but not in PC12 cells (Fig. 3 and Supplementary Fig. S3). The CB6's inhibition effects on the MTORC1 pathway depend on different cell types, concentrations, and durations of the treatment. In addition, hyperactivation of MTORC1 signaling by knocking down *TSC2* did not affect the CB6-induced autophagy (Supplementary Fig. S3). Therefore, CB6 may inhibit MTORC1 signaling at high concentrations. However, CB6-

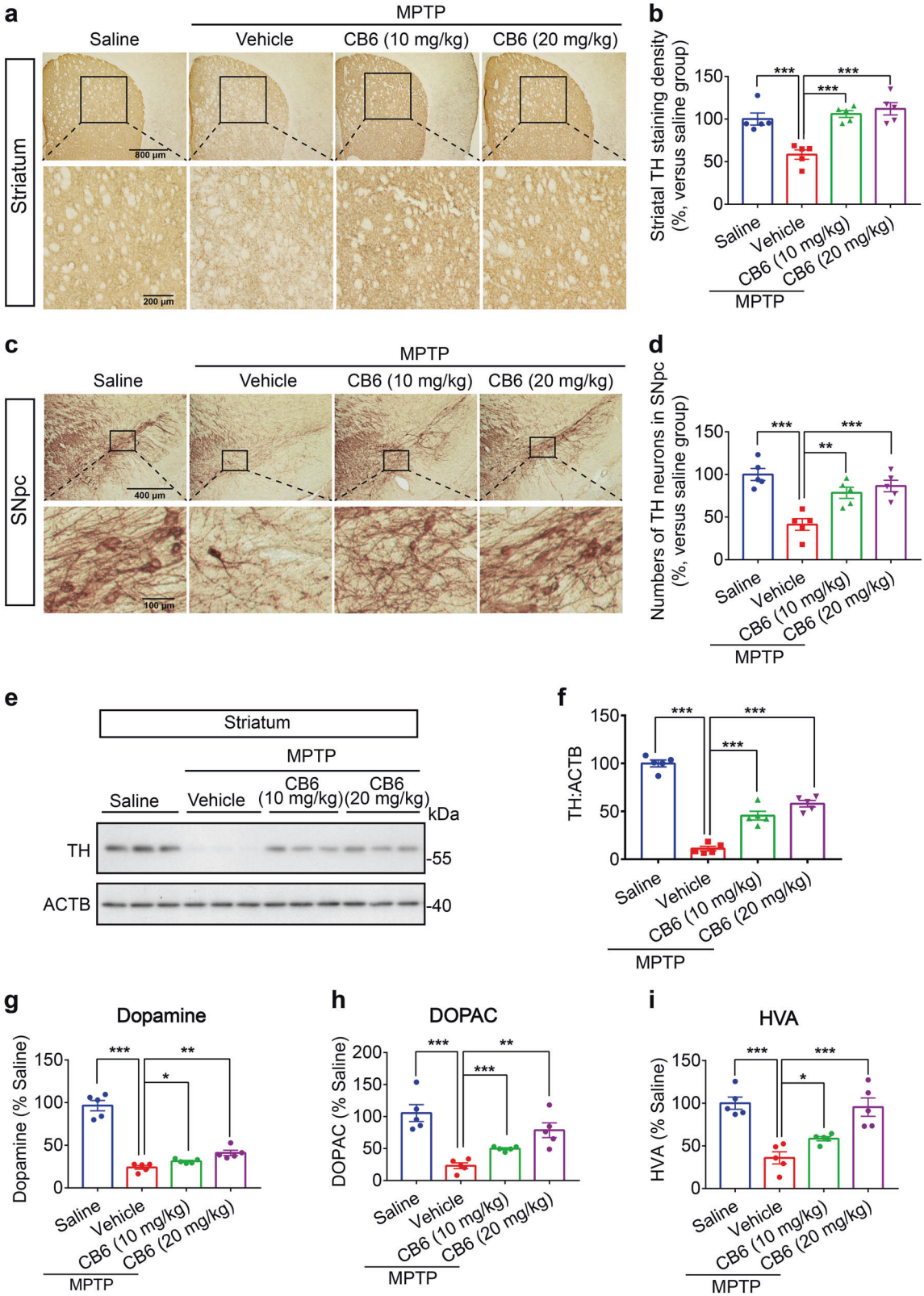


**Fig. 10 CB6 protects dopaminergic neurons in an MPTP mouse model of PD.** Representative DAB-staining images of tyrosine hydroxylase (TH)-positive dopaminergic neurons in the striatum (**a**) and substantia nigra pars compacta (SNpc) (**c**) of mouse brains. Statistical results for the relative density of TH in the striatum (**b**) and the relative number of TH-positive neurons in the SNpc (**d**). Data were quantified as mean ± SEM ($n = 5$). $^{**}P < 0.01$ and $^{***}P < 0.001$ vs. MPTP group. **e** Representative Western blots show the levels of TH in the striatum of mouse brains. **f** The relative levels of TH in the striatum were quantified as mean ± SEM ($n = 5$). $^{***}P < 0.001$ vs. MPTP group. **g–i** Representative images show the levels of dopamine, 3,4-dihydroxyphenylacetic acid (DOPAC), and homovanillic acid (HVA) in the striatum of mouse brains. Dopamine, DOPAC, and HVA were extracted in 80% methanol in $ddH_2O$, determined by LC-MS/MS analysis, and calculated. Data were quantified as mean ± SEM ($n = 5$). $^{*}P < 0.05$, $^{**}P < 0.01$ and $^{***}P < 0.001$ vs. MPTP group.

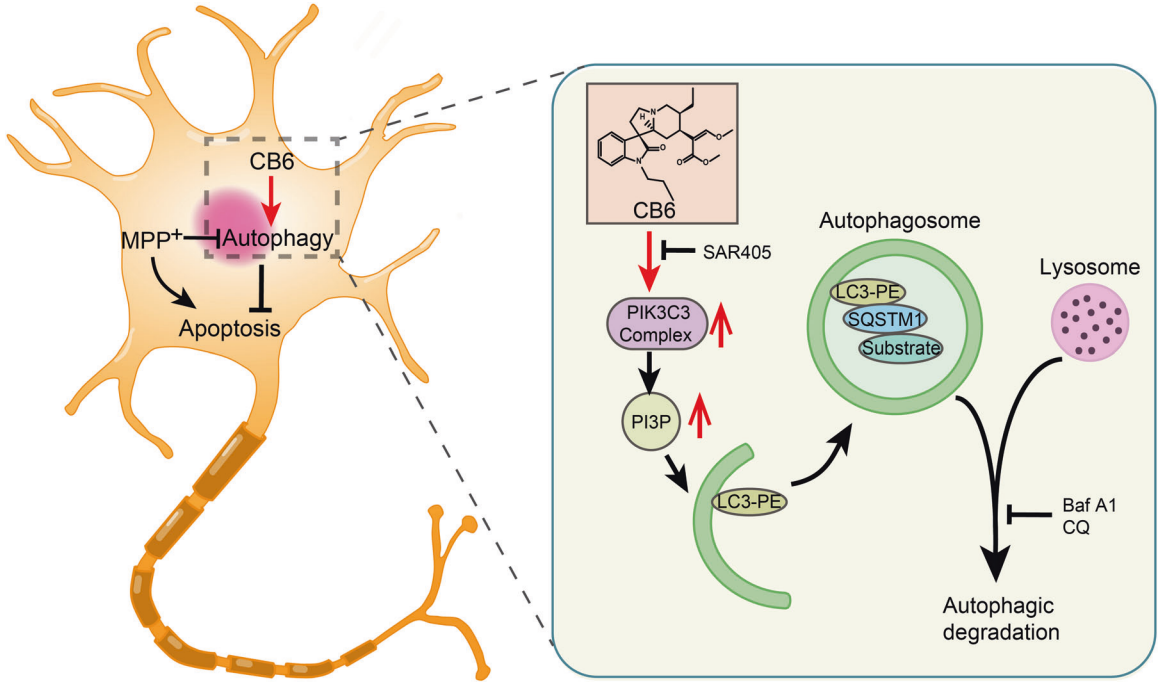


**Fig. 11 A mechanistic model shows that CB6 inhibits $MPP^+$-induced apoptosis in neural cells involving the activation of PIK3C3 complex-dependent autophagy.** In vitro findings suggest that CB6 treatment enhances the activity of the PIK3C3 complex and the production of PI3P, thereby promoting the lipidation of LC3B and accelerating autophagic degradation, which may contribute to the neuroprotection of CB6 against $MPP^+$-induced apoptosis in dopaminergic neurons.

induced autophagy is independent of the MTORC1 pathway, which is consistent with Cory B.

PD is a progressive neurodegenerative disease, characterized by the loss of dopaminergic neurons in the SNpc. PD-associated mutations are primarily involved in autophagy impairment [6]. For example, mutations in PTEN-induced kinase 1 (PINK1) are associated with autosomal recessive PD [45]. Normal full-length PINK1 interacts with BECN1 and enhances PIK3C3 complex-dependent autophagy, whereas PINK1 mutant W437X fails to interact with BECN1, leading to autophagy dysfunction in PD [46]. As the PIK3C3 complex plays a crucial role in the initiation of autophagy [47], activation of the PIK3C3 complex is a feasible solution to induce autophagy in the treatment of PD. Studies have shown that overexpression of SLC35D3, which is selectively expressed in midbrain dopaminergic neurons, enhances the formation of BECN1-ATG14-PIK3C3 complex, thus activating autophagy and preventing the loss of dopaminergic neurons [48]. However, small molecules which enhance the activity of the PIK3C3 complex in the treatment of PD are still unavailable. In this study, we report a synthesized alkaloid CB6 enhances the activity of PIK3C3 complex, thus inducing autophagy and protecting neurons in PD models.

Overall, CB6 has good brain permeability and has autophagy-inducing and neuroprotective effects by activating the PIK3C3 complex, making it an orally effective drug candidate for the prevention or treatment of PD.

## ACKNOWLEDGEMENTS

We thank Roy Chun-laam Ng (The University of Hong Kong) and Karen Wong (The University of Hong Kong) for processing TEM samples; Zi-wan Ning (Hong Kong Baptist University) for performing pharmacokinetic analysis; Xiao-jian Shao (Hong Kong Baptist University) for analyzing LC-MS/MS data; and Dr. Martha Dahlen for the English editing. This study was supported by Hong Kong General Research Fund (GRF/HKBU12100618, GRF/HKBU12101417), the National Natural Science Foundation of China (81703487, 81773926), Shenzhen Science and Technology Innovation Commission (JCYJ20180507184656626, JCYJ20180302174028790), Hong Kong Health and Medical Research Fund (HMRF17182541, HMRF17182551, HMRF-17182561), and Research Fund from Hong Kong Baptist University (HKBU/RC-IRCs/17-18/03, IRCMS/19-20/H02, GDS-84/506/2019).

## AUTHOR CONTRIBUTIONS

JXS and ML designed the research; ZZ, LFL, CFS, JL, SGS, XJG, and YXK performed the main experiments; WJX and CLZ synthesized the compound CB6; ZZ, BCKT, AI, and SK analyzed the data; ZZ and JXS wrote the paper; ZZ, KHC, JHL, JQT, HJZ, JXS, and ML revised the paper; JXS and ML supervised the study.

## ADDITIONAL INFORMATION

**Supplementary information** The online version contains supplementary material available at https://doi.org/10.1038/s41401-022-00871-0.

**Competing interests:** The authors declare no competing interests.

## REFERENCES

1. Sveinbjornsdottir S. The clinical symptoms of Parkinson's disease. J Neurochem. 2016;139:318–24.
2. Charvin D, Medori R, Hauser RA, Rascol O. Therapeutic strategies for Parkinson disease: beyond dopaminergic drugs. Nat Rev Drug Discov. 2018;17:804–22.
3. Athauda D, Foltynie T. The ongoing pursuit of neuroprotective therapies in Parkinson disease. Nat Rev Neurol. 2015;11:25–40.
4. Mizushima N. Autophagy: process and function. Genes Dev. 2007;21:2861–73.
5. Doherty J, Baehrecke EH. Life, death and autophagy. Nat Cell Biol. 2018;20:1110–7.
6. Boland B, Yu WH, Corti O, Mollereau B, Henriques A, Bezard E, et al. Promoting the clearance of neurotoxic proteins in neurodegenerative disorders of ageing. Nat Rev Drug Discov. 2018;17:660–88.
7. Karabiyik C, Lee MJ, Rubinsztein DC. Autophagy impairment in Parkinson's disease. Essays Biochem. 2017;61:711–20.
8. Anglade P, Vyas S, Javoy-Agid F, Herrero MT, Michel PP, Marquez J, et al. Apoptosis and autophagy in nigral neurons of patients with Parkinson's disease. Histol Histopathol. 1997;12:25–31.
9. Moors TE, Paciotti S, Ingrassia A, Quadri M, Breedveld G, Tasegian A, et al. Characterization of brain lysosomal activities in GBA-related and sporadic Parkinson's disease and dementia with Lewy bodies. Mol Neurobiol. 2019;56:1344–55.
10. Webb JL, Ravikumar B, Atkins J, Skepper JN, Rubinsztein DC. Alpha-Synuclein is degraded by both autophagy and the proteasome. J Biol Chem. 2003;278:25009–13.

11. Winslow AR, Rubinsztein DC. The Parkinson disease protein alpha-synuclein inhibits autophagy. Autophagy. 2011;7:429–31.
12. Madureira M, Connor-Robson N, Wade-Martins R. LRRK2: autophagy and lysosomal activity. Front Neurosci. 2020;14:498.
13. Zavodszky E, Seaman MN, Moreau K, Jimenez-Sanchez M, Breusegem SY, Harbour ME, et al. Mutation in VPS35 associated with Parkinson's disease impairs WASH complex association and inhibits autophagy. Nat Commun. 2014;5:3828.
14. Komatsu M, Waguri S, Chiba T, Murata S, Iwata J, Tanida I, et al. Loss of autophagy in the central nervous system causes neurodegeneration in mice. Nature. 2006;441:880–4.
15. Hara T, Nakamura K, Matsui M, Yamamoto A, Nakahara Y, Suzuki-Migishima R, et al. Suppression of basal autophagy in neural cells causes neurodegenerative disease in mice. Nature. 2006;441:885–9.
16. Djajadikerta A, Keshri S, Pavel M, Prestil R, Ryan L, Rubinsztein DC. Autophagy induction as a therapeutic strategy for neurodegenerative diseases. J Mol Biol. 2020;432:2799–821.
17. Menzies FM, Fleming A, Rubinsztein DC. Compromised autophagy and neurodegenerative diseases. Nat Rev Neurosci. 2015;16:345–57.
18. Liu LF, Song JX, Lu JH, Huang YY, Zeng Y, Chen LL, et al. Tianma Gouteng Yin, a Traditional Chinese Medicine decoction, exerts neuroprotective effects in animal and cellular models of Parkinson's disease. Sci Rep. 2015;5:16862.
19. Sakakibara I, Terabayashi S, Kubo M, Higuchi M, Komatsu Y, Okada M, et al. Effect on locomotion of indole alkaloids from the hooks of uncaria plants. Phytomedicine. 1999;6:163–8.
20. Lu JH, Tan JQ, Durairajan SS, Liu LF, Zhang ZH, Ma L, et al. Isorhynchophylline, a natural alkaloid, promotes the degradation of alpha-synuclein in neuronal cells via inducing autophagy. Autophagy. 2012;8:98–108. (Erratum in Autophagy. 2012; 8(5): 864–6.)
21. Chen LL, Wang YB, Song JX, Deng WK, Lu JH, Ma LL, et al. Phosphoproteome-based kinase activity profiling reveals the critical role of MAP2K2 and PLK1 in neuronal autophagy. Autophagy. 2017;13:1969–80.
22. Song JX, Lu JH, Liu LF, Chen LL, Durairajan SS, Yue Z, et al. HMGB1 is involved in autophagy inhibition caused by SNCA/alpha-synuclein overexpression: a process modulated by the natural autophagy inducer corynoxine B. Autophagy. 2014;10:144–54.
23. Tanida I, Ueno T, Kominami E. LC3 conjugation system in mammalian autophagy. Int J Biochem Cell Biol. 2004;36:2503–18.
24. Pankiv S, Clausen TH, Lamark T, Brech A, Bruun JA, Outzen H, et al. p62/SQSTM1 binds directly to Atg8/LC3 to facilitate degradation of ubiquitinated protein aggregates by autophagy. J Biol Chem. 2007;282:24131–45.
25. Liu Q, Chang JW, Wang J, Kang SA, Thoreen CC, Markhard A, et al. Discovery of 1-(4-(4-propionylpiperazin-1-yl)-3-(trifluoromethyl)phenyl)-9-(quinolin-3-yl)benzo[h][1,6] naphthyridin-2(1H)-one as a highly potent, selective mammalian target of rapamycin (mTOR) inhibitor for the treatment of cancer. J Med Chem. 2010;53:7146–55.
26. Liu Q, Kirubakaran S, Hur W, Niepel M, Westover K, Thoreen CC, et al. Kinome-wide selectivity profiling of ATP-competitive mammalian target of rapamycin (mTOR) inhibitors and characterization of their binding kinetics. J Biol Chem. 2012;287:9742–52.
27. Tanida I, Yamasaki M, Komatsu M, Ueno T. The FAP motif within human ATG7, an autophagy-related E1-like enzyme, is essential for the E2-substrate reaction of LC3 lipidation. Autophagy. 2012;8:88–97.
28. Klionsky DJ, Abdel-Aziz AK, Abdelfatah S, Abdellatif M, Abdoli A, Abel S, et al. Guidelines for the use and interpretation of assays for monitoring autophagy (4th edition)(1). Autophagy. 2021;17:1–382.
29. Zhu Z, Yang C, Iyaswamy A, Krishnamoorthi S, Sreenivasmurthy SG, Liu J, et al. Balancing mTOR signaling and autophagy in the treatment of Parkinson's disease. Int J Mol Sci. 2019;20:728.
30. Nojima H, Tokunaga C, Eguchi S, Oshiro N, Hidayat S, Yoshino K, et al. The mammalian target of rapamycin (mTOR) partner, raptor, binds the mTOR substrates p70 S6 kinase and 4E-BP1 through their TOR signaling (TOS) motif. J Biol Chem. 2003;278:15461–4.
31. Nascimbeni AC, Codogno P, Morel E. Phosphatidylinositol-3-phosphate in the regulation of autophagy membrane dynamics. FEBS J. 2017;284:1267–78.
32. Dooley HC, Wilson MI, Tooze SA. WIPI2B links PtdIns3P to LC3 lipidation through binding ATG16L1. Autophagy. 2015;11:190–1.
33. Pasquier B. SAR405, a PIK3C3/Vps34 inhibitor that prevents autophagy and synergizes with MTOR inhibition in tumor cells. Autophagy. 2015;11:725–6.
34. Nascimbeni AC, Codogno P, Morel E. Local detection of PtdIns3P at autophagosome biogenesis membrane platforms. Autophagy. 2017;13:1602–12.
35. Feng Y, He D, Yao Z, Klionsky DJ. The machinery of macroautophagy. Cell Res. 2014;24:24–41.
36. Lu J, He L, Behrends C, Araki M, Araki K, Jun Wang Q, et al. NRBF2 regulates autophagy and prevents liver injury by modulating Atg14L-linked phosphatidylinositol-3 kinase III activity. Nat Commun. 2014;5:3920.
37. Itakura E, Kishi C, Inoue K, Mizushima N. Beclin 1 forms two distinct phosphatidylinositol 3-kinase complexes with mammalian Atg14 and UVRAG. Mol Biol Cell. 2008;19:5360–72.
38. Zeng X, Chen J, Deng X, Liu Y, Rao MS, Cadet JL, et al. An in vitro model of human dopaminergic neurons derived from embryonic stem cells: $MPP^+$ toxicity and GDNF neuroprotection. Neuropsychopharmacology. 2006;31:2708–15.
39. Langston JW, Irwin I, Langston EB, Forno LS. 1-Methyl-4-phenylpyridinium ion ($MPP^+$): identification of a metabolite of MPTP, a toxin selective to the substantia nigra. Neurosci Lett. 1984;48:87–92.
40. Liu Y, Jin W, Deng Z, Zhang Q, Wang J, Glucuronomannan GM2 from Saccharina japonica enhanced mitochondrial function and autophagy in a Parkinson's model. Mar Drugs. 2021;19:58.
41. Kaul S, Kanthasamy A, Kitazawa M, Anantharam V, Kanthasamy AG. Caspase-3 dependent proteolytic activation of protein kinase C delta mediates and regulates 1-methyl-4-phenylpyridinium ($MPP^+$)-induced apoptotic cell death in dopaminergic cells: relevance to oxidative stress in dopaminergic degeneration. Eur J Neurosci. 2003;18:1387–401.
42. Su Z, Yang Z, Xu Y, Chen Y, Yu Q. Apoptosis, autophagy, necroptosis, and cancer metastasis. Mol Cancer. 2015;14:48.
43. Jackson-Lewis V, Przedborski S. Protocol for the MPTP mouse model of Parkinson's disease. Nat Protoc. 2007;2:141–51.
44. Yan D, Ma Z, Liu C, Wang C, Deng Y, Liu W, et al. Corynoxine B ameliorates HMGB1-dependent autophagy dysfunction during manganese exposure in SH-SY5Y human neuroblastoma cells. Food Chem Toxicol. 2019;124:336–48.
45. Criscuolo C, Volpe G, De Rosa A, Varrone A, Marongiu R, Mancini P, et al. PINK1 homozygous W437X mutation in a patient with apparent dominant transmission of parkinsonism. Mov Disord. 2006;21:1265–7.
46. Michiorri S, Gelmetti V, Giarda E, Lombardi F, Romano F, Marongiu R, et al. The Parkinson-associated protein PINK1 interacts with Beclin1 and promotes autophagy. Cell Death Differ. 2010;17:962–74.
47. Rostislavleva K, Soler N, Ohashi Y, Zhang L, Pardon E, Burke JE, et al. Structure and flexibility of the endosomal Vps34 complex reveals the basis of its function on membranes. Science. 2015;350:aac7365.
48. Wei ZB, Yuan YF, Jaouen F, Ma MS, Hao CJ, Zhang Z, et al. SLC35D3 increases autophagic activity in midbrain dopaminergic neurons by enhancing BECN1-ATG14-PIK3C3 complex formation. Autophagy. 2016;12:1168–79.